Reducing Exact Two-Component Theory for NMR Couplings to a One-Component Approach: Efficiency and Accuracy

Yannick J. Franzke*

Fachbereich Chemie, Philipps-Universität Marburg, Hans-Meerwein-Str. 4, 35032 Marburg, Germany

E-mail: yannick.franzke@chemie.uni-marburg.de

Abstract

The self-consistent and complex spin–orbit exact two-component (X2C) formalism for NMR spin–spin coupling constants [J. Chem. Theory Comput. **17**, 3974–3994 (2021)] is reduced to a scalar one-component ansatz. This way, the first-order response term can be partitioned into the Fermi-contact (FC) and spin–dipole (SD) interactions as well as the paramagnetic spin–orbit (PSO) contribution. The FC+SD terms are real and symmetric, while the PSO term is purely imaginary and antisymmetric. The relativistic one-component approach is combined with a modern density functional treatment up to local hybrid functionals including the response of the current density. Computational demands are reduced by factors of 8–24 as shown for a large tin compound consisting of 137 atoms. Limitations of the current ansatz are critically assessed, i.e. the one-component treatment is not sufficient for tin compounds featuring a few heavy halogen atoms.

1 Introduction

Nuclear magnetic resonance (NMR) spectroscopy is an indispensable tool for organic, inorganic, and organometallic chemistry. NMR spectra can be measured for almost all elements and provide important information about the chemical environment.[1–7] An accurate theoretical framework beyond the third row of the periodic table of elements necessitates the inclusion of special relativity.[8–25] For instance, it was shown that selenium and tin NMR spectra are substantially affected by relativistic effects.[26–35] This holds for both the chemical shift, describing the position of the signal, and the indirect spin–spin coupling constant (SSCC), describing the multiplet pattern.

Relativistic effects can be treated at different levels of accuracy.[17–25] The most straightforward and most accurate choice is a four-component (4c) framework directly based on the many-electron Dirac–Coulomb equation. This was also successfully applied to NMR coupling constants.[36–39] However, this leads to comparably high computational costs, as both the electronic and the so-called positronic states are described. Relativistic two-component (2c) approaches aim at decoupling[40,41] these states to arrive at an electrons-only Hamiltonian.[19–25] Popular ansätze for these 2c frameworks are the zeroth-order regular approximation[42–44] (ZORA) and (one-electron) exact two-component (X2C) theory.[45–51] As indicated by the names, X2C is formally more accurate. Two-component approaches describe both scalar-relativistic and spin–orbit effects self-consistently, and complex algebra is still needed. Computational demands may be further reduced by scalar one-component (1c) approaches, which can be implemented with real matrices and algebra only. For ZORA, both a 1c and a 2c formalism were presented for NMR coupling constants.[52–55] In contrast, the X2C Hamiltonian is so far exclusively used in its complex spin–orbit fashion for NMR couplings.[56–58]

Herein, I will present a scalar X2C ansatz for NMR coupling constants, and assess its efficiency and accuracy. This is motivated by the following thoughts. First, a one-component formalism is substantially less demanding for both the self-consistent field (SCF) procedure and the NMR calculation. Converging the 2c ground-state density is technically more in-

volved than its 1c counter part. Second, a relativistic one-component Hamiltonian can be directly interfaced to the existing non-relativistic code machinery. Therefore, one-component methods will address a broader community in terms of quantum chemical program suites. Third, a one-component approach allows for a simpler interpretation of the results regrading the different contributions to the NMR coupling constant.

The theory for such a one-component approach is described in Section 2. Computational methods and results for its application to main-group organometallic chemistry are discussed in Sections 3 and 4. The work is summarized in Section 5, where the conclusions are drawn.

2 Theory and Implementation

To illustrate how the self-consistent and complex two-component approach is truncated to a one-component ansatz, I first review the non-relativistic one-component and the relativistic two-component approaches based on the definition of the NMR coupling tensor. In SI units, the nuclear spin–spin coupling tensor $\mathbf{J}_{M,N}$ of the nuclei M and N is defined as

$$\left(\mathbf{J}_{M,N}\right)_{u,v} = h\frac{\gamma_M}{2\pi}\frac{\gamma_N}{2\pi}\left(\mathbf{K}_{M,N}\right)_{u,v} \tag{1}$$

with the reduced indirect spin–spin coupling tensor $\mathbf{K}_{M,N}$. γ_M is the gyromagnetic ratio of the nucleus M.[59,60] The reduced coupling tensor $\mathbf{K}_{M,N}$ is simply the derivative of the electronic energy E with respect to the corresponding nuclear magnetic moments $\vec{m}_M$ and $\vec{m}_N$. This derivative is formed in the limit of a vanishing perturbation, e.g. $m_{M,u} = 0$. u and v denote the Cartesian indices. The isotropic coupling constant $J(M,N)$ or J_{MN} describing the splitting of the signals in the NMR spectra is a third of the trace,

$$J(M,N) = \frac{1}{3}\sum_u \left(\mathbf{J}_{M,N}\right)_{u,u} \tag{2}$$

2.1 Non-Relativistic Theory

The non-relativistic theory was formulated by Ramsey.[61] Here, the coupling is described with the Fermi-contact (FC), spin–dipole (SD), paramagnetic spin–orbit (PSO), and the diamagnetic spin–orbit (DSO) operators according to

$$h^{\mathrm{FC}} = \frac{8\pi}{3c^2} \sum_{i,M} \delta(\vec{r}_{iM})\ \vec{s}_i \cdot \vec{m}_M \tag{3}$$

$$h^{\mathrm{SD}} = \frac{1}{c^2} \sum_{i,M} \frac{3\,(\vec{s}_i \cdot \vec{r}_{iM})\,(\vec{m}_i \cdot \vec{r}_{iM}) - r_{iM}^2 \vec{s}_i \cdot \vec{m}_M}{r_{iM}^5} \tag{4}$$

$$h^{\mathrm{PSO}} = -\frac{\mathrm{i}}{c^2} \sum_{i,M} \frac{\vec{m}_M \times \vec{r}_{iM}}{r_{iM}^3} \cdot \vec{\nabla}_i \tag{5}$$

$$h^{\mathrm{DSO}} = \frac{1}{c^4} \sum_{i,M,N} \frac{\vec{m}_M \cdot (\vec{r}_{iM} \cdot \vec{r}_{iN})\,\vec{m}_N - (\vec{r}_{iM} \cdot \vec{m}_M)\,(\vec{r}_{iN} \cdot \vec{m}_N)}{r_{iM}^3 r_{iN}^3} \tag{6}$$

Uppercase letters refer to the nuclei and lowercase indices denote the electronic coordinates. c is the speed of light ($c = 137.0359990840\,\mathrm{a.u.}$).[62]

Using the coupled-perturbed Kohn–Sham (CPKS) formalism, these operators allow to compute the coupling tensor according to[4,63–66]

$$\begin{aligned}\mathbf{K}_{M,N} = \mathbf{K}_{M,N}^{\mathrm{DSO}} &+ \sum_{ai} \lambda_{M,ai}^{\mathrm{PSO}} \left(\kappa_{N,ai}^{\mathrm{PSO}}\right)^{\mathrm{T}} + \mathbf{K}_{M,N}^{\mathrm{FC/SD}} \\ &+ \mathbf{1}_3 \sum_{ai} \lambda_{M,ai}^{\mathrm{FC}} \kappa_{N,ai}^{\mathrm{FC}} + \sum_{ai} \lambda_{M,ai}^{\mathrm{SD}} \left(\kappa_{N,ai}^{\mathrm{SD}}\right)^{\mathrm{T}}\end{aligned} \tag{7}$$

Note that $\mathbf{1}_3$ is the (3×3) unit matrix. $\lambda_{M,ai}$ indicates the response of the Kohn–Sham (KS) wavefunction to the perturbation associated with the magnetic moment $\vec{m}_M$. That is, response equations of the type

$$\sum_{bj} G_{ai,bj} \lambda_{M,bj} = -\kappa_{M,ai} \tag{8}$$

are solved. $a, b, \ldots$ denote virtual orbitals, while $i, j, \ldots$ denote occupied orbitals. $G_{ai,bj}$ is

the electronic Hessian including the exchange-correlation kernel.[4,63–71] The right-hand side $\kappa_{M,ai}$ is made up of the one-electron integral derivatives

$$\left(h^{\mathrm{FC}}\right)_u^M = \frac{8\pi}{3c^2} \langle\mu|\delta\left(\vec{r}_M\right)\delta_{uw}|\nu\rangle \tag{9}$$

$$\left(h^{\mathrm{SD}}\right)_u^M = \frac{1}{c^2} \langle\mu|\frac{3r_{M,w}r_{M,u} - r_M^2\delta_{uw}}{r_M^5}|\nu\rangle \tag{10}$$

$$\left(h^{\mathrm{PSO}}\right)_u^M = -\frac{\mathrm{i}}{c^2} \langle\mu|\left(\frac{\vec{r}_M \times \vec{\nabla}}{r_M^3}\right)_u|\nu\rangle \tag{11}$$

being transformed to the molecular orbital (MO) occupied-virtual tensor space (i, a) from the atomic orbital (AO) representation (μ, ν). w is associated with the formal spin state (spin x, y, z), δ_{uw} indicates the Kronecker delta, and $\delta(\vec{r}_M)$ the delta distribution. A shorthand notation is employed to indicate derivatives with respect to the nuclear magnetic moments, i.e. $\left(h^{\mathrm{PSO}}\right)_u^M = \partial h^{\mathrm{PSO}}/\partial m_{M,u}$. The FC and SD terms are real and symmetric, i.e. they correspond to singlet exciations.[4] In contrast, the PSO integrals are purely imaginary and antisymmetric, corresponding to triplet excitations.[4] This means that there are one response equation for the FC term, six equations for the SD term (due to symmetry), and three equations for the PSO term to be solved. For the DSO term, no response equations are needed and the integral derivatives

$$\left(h^{\mathrm{DSO}}\right)_{M,N}^{u,v} = \frac{1}{c^4} \langle\mu|\frac{\delta_{uv}\vec{r}_M \cdot \vec{r}_N - r_{N,u}r_{M,v}}{r_M^3 r_N^3}|\nu\rangle \tag{12}$$

are directly contracted with the ground-state density matrix. $\mathbf{K}_{M,N}^{\mathrm{FC/SD}}$ is the FC-SD cross contribution to the anisotropy

$$\mathbf{K}_{M,N}^{\mathrm{FC/SD}} = \sum_{ai} \lambda_{M,ai}^{\mathrm{FC}}\kappa_{N,ai}^{\mathrm{SD}} + \sum_{ai} \kappa_{M,ai}^{\mathrm{SD}}\lambda_{N,ai}^{\mathrm{FC}} \tag{13}$$

$$= \sum_{ai} \lambda_{M,ai}^{\mathrm{FC}}\kappa_{N,ai}^{\mathrm{SD}} + \sum_{ai} \lambda_{M,ai}^{\mathrm{SD}}\kappa_{N,ai}^{\mathrm{FC}} \tag{14}$$

See, e.g., refs. 4 and 66 for more details.

2.2 Exact Two-Component Theory

In the spin–orbit two-component X2C formalism,[56–58] the derivatives of the one-electron Hamiltonians are obtained by decoupling the energy sub-spaces of the one-electron Dirac equation in a restricted kinetically based basis set,[72]

$$\left|\psi_p^{\mathrm{L}}\right\rangle = \sum_{\mu} c_{\mu p}^{\mathrm{L}} \left|\mu\right\rangle \tag{15}$$

$$\left|\psi_p^{\mathrm{S}}\right\rangle = \sum_{\mu} c_{\mu p}^{\mathrm{S}} \frac{\vec{\sigma}\cdot\vec{p}}{2c} \left|\mu\right\rangle \tag{16}$$

$$\begin{pmatrix} \mathbf{V} & \mathbf{\Pi}^{\dagger} \\ \mathbf{\Pi} & (\frac{1}{4c^2}\mathbf{W} - \mathbf{T}) \end{pmatrix} \begin{pmatrix} \mathbf{C}_-^{\mathrm{L}} & \mathbf{C}_+^{\mathrm{L}} \\ \mathbf{C}_-^{\mathrm{S}} & \mathbf{C}_+^{\mathrm{S}} \end{pmatrix} = \begin{pmatrix} \mathbf{S} & \mathbf{0}_2 \\ \mathbf{0}_2 & \frac{1}{2c^2}\mathbf{T} \end{pmatrix} \begin{pmatrix} \mathbf{C}_-^{\mathrm{L}} & \mathbf{C}_+^{\mathrm{L}} \\ \mathbf{C}_-^{\mathrm{S}} & \mathbf{C}_+^{\mathrm{S}} \end{pmatrix} \begin{pmatrix} \boldsymbol{\epsilon}_- & \mathbf{0}_2 \\ \mathbf{0}_2 & \boldsymbol{\epsilon}_+ \end{pmatrix} \tag{17}$$

$+$ and $-$ denote the electronic and positronic states of the energy $\boldsymbol{\epsilon}_+$ and $\boldsymbol{\epsilon}_-$. $\mathbf{C}^{\mathrm{L}}$ and $\mathbf{C}^{\mathrm{S}}$ are the respective eigenvectors of the large (L) and small (S) component. The Dirac matrix on the left-hand side of eq. 17 consists of one-electron integrals. In the (2×2) super-space, the overlap matrix $\mathbf{S}$, kinetic energy matrix $\mathbf{T}$, and potential matrix $\mathbf{V}$ read

$$\mathbf{S} = \begin{pmatrix} \mathbf{S}^0 & \mathbf{0} \\ \mathbf{0} & \mathbf{S}^0 \end{pmatrix}, \quad \mathbf{S}_{\mu\nu}^0 = \langle\mu|\nu\rangle \tag{18}$$

$$\mathbf{T} = \begin{pmatrix} \mathbf{T}^0 & \mathbf{0} \\ \mathbf{0} & \mathbf{T}^0 \end{pmatrix}, \quad \mathbf{T}_{\mu\nu}^0 = \langle\mu|\frac{1}{2}p^2|\nu\rangle \tag{19}$$

$$\mathbf{V} = \begin{pmatrix} \mathbf{V}^0 & \mathbf{0} \\ \mathbf{0} & \mathbf{V}^0 \end{pmatrix}, \quad \mathbf{V}_{\mu\nu}^0 = \langle\mu|V|\nu\rangle \tag{20}$$

Only the relativistically modified potential $\mathbf{W}$ and the generalized momentum matrix $\mathbf{\Pi}$ include the electron spin via the Pauli spin matrices, $\vec{\sigma} = (\sigma_x, \sigma_y, \sigma_z)$, according to

$$\mathbf{W}_{\mu\nu} = \langle\mu|(\vec{\sigma}\cdot\vec{p})\, V\, (\vec{\sigma}\cdot\vec{p})|\nu\rangle \tag{21}$$

$$\mathbf{\Pi}^{\dagger}_{\mu\nu} = \frac{1}{2c} \langle \mu | c\ \vec{\sigma} \cdot \left(\vec{p} + \frac{1}{c} \vec{A} \right) | (\vec{\sigma} \cdot \vec{p})\ \nu \rangle \tag{22}$$

$\vec{A}$ is the vector potential of the nuclear magnetic moments, which was introduced via the principle of minimal coupling,[73]

$$\vec{A} = \sum_M \vec{A}_M = \sum_M \frac{\vec{m}_M \times \vec{r}_M}{r_M^3} \tag{23}$$

The point-charge model for the vector potential was assumed for comparison with the non-relativistic integrals. The generalization to the finite nucleus model is straightforward.[74–78]

Application of the one-electron X2C decoupling scheme,[45–51] results in the electrons-only Hamiltonian

$$\mathbf{h}^{+} = \mathbf{R}^{\dagger} \mathbf{L} \mathbf{R} \tag{24}$$

$\mathbf{L}$ is the so-called normalized-elimination-of-the-small-component (NESC) matrix.[79–82] The decoupling matrix $\mathbf{X}$ and the renormalization matrix $\mathbf{R}$ read

$$\mathbf{X} = \mathbf{C}^{\mathrm{S}}_{+} (\mathbf{C}^{\mathrm{L}}_{+})^{-1} \tag{25}$$

$$\mathbf{R} = \mathbf{S}^{-1/2} \left(\mathbf{S}^{-1/2} \tilde{\mathbf{S}} \mathbf{S}^{-1/2} \right)^{-1/2} \mathbf{S}^{1/2} \tag{26}$$

$$\tilde{\mathbf{S}} = \mathbf{S} + \frac{1}{2c^2} \mathbf{X}^{\dagger} \mathbf{T} \mathbf{X} \tag{27}$$

Analytical derivative theory[19,21] for eq. 1, leads to the derivative of the X2C Hamiltonian

$$\mathbf{h}^{+,M}_{u} = \mathbf{R}^{\dagger,M}_{u} \mathbf{L} \mathbf{R} + \mathbf{R}^{\dagger} \mathbf{L}^{M}_{u} \mathbf{R} + \mathbf{R}^{\dagger} \mathbf{L} \mathbf{R}^{M}_{u} \tag{28}$$

with the derivative of the NESC matrix

$$\begin{aligned} \mathbf{L}^{M}_{u} = & \mathbf{X}^{\dagger,M}_{u} \mathbf{T} + \mathbf{X}^{\dagger} \mathbf{\Pi}^{M}_{u} + \mathbf{\Pi}^{\dagger,M}_{u} \mathbf{X} + \mathbf{T} \mathbf{X}^{M}_{u} \\ & + \mathbf{X}^{\dagger,M}_{u} \left(\frac{1}{4c^2} \mathbf{W} - \mathbf{T} \right) \mathbf{X} + \mathbf{X}^{\dagger} \left(\frac{1}{4c^2} \mathbf{W} - \mathbf{T} \right) \mathbf{X}^{M}_{u} \end{aligned} \tag{29}$$

This equation involves the one-electron integral derivatives for the generalized momentum matrix given by[56,57]

$$\left(\mathbf{\Pi}^{\dagger}_{\mu\nu}\right)^{M}_{u} = \frac{1}{2c}\left\langle\mu\right|\left(\frac{\vec{r}_M}{r^3_M}\times\vec{\sigma}\right)_u\left|(\vec{\sigma}\cdot\vec{p})\,\nu\right\rangle \tag{30}$$

Recipes to calculate the derivative of the decoupling and the renormalization matrix can be found in the literature.[78,83–86] Due to spin–orbit effects the FC, SD, and PSO terms are coupled and only three complex response equations are solved in the spinor space.[87]

In restricted kinetic balance (RKB), the unperturbed density or DSO contribution only arises due to the second-order one-electron X2C response equations.[56,57] The respective second-order integral derivatives of $\mathbf{\Pi}$ are zero. We note in passing that a restricted magnetically balanced (RMB) basis set is used in four-component approaches according to[39]

$$\left|\psi^{\mathrm{L}}_p\right\rangle = \sum_{\mu} c^{\mathrm{L}}_{\mu p}\left|\mu\right\rangle \tag{31}$$

$$\left|\psi^{\mathrm{S}}_p\right\rangle = \sum_{\mu} c^{\mathrm{S}}_{\mu p}\frac{\vec{\sigma}\cdot\vec{\pi}}{2c}\left|\mu\right\rangle \tag{32}$$

with $\vec{\pi} = \vec{p} + \frac{1}{c}\vec{A}$. However, this is problematic in one-electron X2C[56] and the kinetic balance only leads to a small deviation when using the spin–orbit X2C response for second-order derivatives.[57]

2.3 One-Component Relativistic Approach

In order to arrive at a one-component formalism, we partition the generalized momentum matrix derivative $\left(\mathbf{\Pi}^{\dagger}_{\mu\nu}\right)^{M}_{u}$ into the spin-dependent and spin-independent contributions according to[88]

$$\left(\mathbf{\Pi}^{\dagger}_{\mu\nu}\right)^{M}_{u} = -\frac{\mathrm{i}}{2c}\left\langle\mu\right|\left(\frac{\vec{r}_M\times\vec{\nabla}}{r^3_M}\right)_u\left|\nu\right\rangle\mathbf{1}_2 + \frac{1}{2c}\left\langle\mu\right|\frac{\vec{\sigma}\cdot\vec{r}_M}{r^3_M}\vec{\nabla}_u - \sigma_u\frac{\vec{r}_M\cdot\vec{\nabla}}{r^3_M}\left|\nu\right\rangle \tag{33}$$

The first term is spin-independent and consists of the non-relativistic PSO integrals, cf. eqs. 5 and 11. Therefore, the PSO contribution to the first-order integral derivatives is extracted in this way. The relativistically modified potential also has to be reduced to its scalar contribution according to

$$\boldsymbol{W} = \begin{pmatrix} \mathbf{W}^0 + \mathrm{i}\mathbf{W}^z & \mathbf{W}^y + \mathrm{i}\mathbf{W}^x \\ -\mathbf{W}^y + \mathrm{i}\mathbf{W}^x & \mathbf{W}^0 - \mathrm{i}\mathbf{W}^z \end{pmatrix} \tag{34}$$

with the real symmetric matrix $\mathbf{W}^0$ and the real antisymmetric matrices $\mathbf{W}^x$, $\mathbf{W}^y$, and $\mathbf{W}^z$

$$\mathbf{W}^0_{\mu\nu} = \langle\mu|p_x V p_x + p_y V p_y + p_z V p_z|\nu\rangle \tag{35}$$

$$\mathbf{W}^x_{\mu\nu} = \langle\mu|p_y V p_z - p_z V p_y|\nu\rangle \tag{36}$$

$$\mathbf{W}^y_{\mu\nu} = \langle\mu|p_z V p_x - p_x V p_z|\nu\rangle \tag{37}$$

$$\mathbf{W}^z_{\mu\nu} = \langle\mu|p_x V p_y - p_y V p_x|\nu\rangle \tag{38}$$

For the one-component ansatz, only $\mathbf{W}^0$ is needed. Constructing the X2C Hamiltonian derivative according to eq. 28 with the spin-independent parts, therefore, only leads to the relativistic PSO term with the same symmetry properties as in the non-relativistic ansatz. The one-component X2C Hamiltonian derivative is obtained by replacing $\mathbf{T}$ and $\mathbf{W}$ in Eq. 28 with $\mathbf{T}^0$ and $\mathbf{W}^0$.

The spin-dependent part of eq. 33, constitutes the FC and SD interaction with

$$\left(\mathbf{\Pi}^{\dagger,\mathrm{FC+SD}}_{\mu\nu}\right)^M_u = \frac{1}{2c}\langle\mu|\frac{\vec{\sigma}\cdot\vec{r}_M}{r_M^3}\vec{\nabla}_u - \sigma_u\frac{\vec{r}_M\cdot\vec{\nabla}}{r_M^3}|\nu\rangle = \frac{1}{2c}\langle\mu|\sum_w\left(\frac{\sigma_w\ r_{M,w}}{r_M^3}\vec{\nabla}_u - \delta_{uw}\sigma_w\frac{\vec{r}_M\cdot\vec{\nabla}}{r_M^3}\right)|\nu\rangle \tag{39}$$

The non-relativistic integrals of Eqs. 9 and 10 are obtained upon integration by parts in the non-relativistic limit,[89] where $\left(\mathbf{\Pi}^{\dagger,\mathrm{FC+SD}}_{\mu\nu}\right)^M_u$ and $\left(\mathbf{\Pi}^{\mathrm{FC+SD}}_{\mu\nu}\right)^M_u$ can simply be added.[90,91] Similar to the spin-dependent part of the relativistically modified potential $\mathbf{W}$ in Eqs. 35–38, $\left(\mathbf{\Pi}^{\dagger,\mathrm{FC+SD}}\right)^M_u$ can be evaluated with three real matrices associated with the spin index

w. This means that we use three matrices for every Cartesian component u, leading to nine matrices in total. These matrices are employed to form the Hamiltonian derivative according to eq. 28. Therefore, nine response equations are solved for the FC+SD terms. The same symmetry considerations and relations to excitations as in the non-relativistic limit are applicable. Thus, this relativistic one-component ansatz, termed SR X2C, leads to a minor computational overhead compared to the non-relativistic approach.

Overall, this one-component approach for the first-order terms is closely related to the one-component formulation of the hyperfine coupling constant in X2C.[90–93] Therefore, this anstatz can be easily implemented by interfacing the respective routines into a non-relativistic implementation of NMR coupling constants.

The DSO term is calculated with the second-order X2C Hamiltonian derivative[78,85,86] using the PSO part of $\mathbf{\Pi}^{\dagger}$ and its derivatives. Therefore, a (3×3) DSO tensor is obtained using $\left(\mathbf{\Pi}^{\mathrm{PSO}}_{\mu\nu}\right)^{M}_{u}$ and $\left(\mathbf{\Pi}^{\mathrm{PSO}}_{\mu\nu}\right)^{N}_{v}$.

2.4 Implementation

The outlined approach was implemented into the TURBOMOLE program suite.[94–97] All required integrals were already available.[57,78,98] Note that we use the finite nucleus model[99] for both the scalar potential and the vector potential. The algorithm for the X2C response part is described in ref. 100 in detail and all steps support the OpenMP paradigm.[101,102] Application of the diagonal local approximation to the unitary decoupling transformation[103,104] (DLU) is straightforward. The reader is referred to Refs. 57, 78, and 98 for details.

The CPKS equations are solved as discussed by Mack *et al.*,[66] with the FC and SD term now being coupled. Additionally, the current density response is included for *meta*-generalized gradient approximations (mGGAs) and local hybrid functionals (see below).[71] The respective magnetic exchange-correlation kernel only affects the PSO term due to symmetry reasons.[69–71] Currently, the implementation supports Hartree–Fock (HF) theory and KS-DFT up to the class of range-separated and local hybrid functionals.

3 Computational Methods

First, the tetrel hydrogen molecules TtH_4 (with Tt = C, Si, Ge, Sn, Pb) are considered, as both 4c RMB results with the BP86 functional[105,106] and experimental findings are available.[39] Structures are taken from ref. 36. The same basis sets and functional as in ref. 39 are applied. That is, an uncontracted Dyall-VTZ basis set (no *g* functions) is used for Ge, Sn, Pb,[107,108] whereas the uncontracted pcJ-2 basis set is employed for C and Si.[109] For comparison, very large girds[110–112] (grid size 5a) are applied for the numerical integration of the DFT contributions. The SCF procedure is converged with thresholds of $10^{-8}\,E_h$ for the total energy and 10^{-8} a.u. for change of the root mean square of the densities. For the CPKS equations, a threshold of 10^{-7} a.u. is chosen for the norm of the residuum. These settings are applied in both one- and two-component calculations based on the DLU-X2C Hamiltonian. In 2c calculations, the modified screened nuclear spin–orbit (mSNSO) approximation[113–115] is further applied. Note that the finite nucleus model for both the scalar potential and the vector potential is used throughout all calculations. The 1c and 2c calculations are carried out with the same program suite in this work, which allows for full consistency.

Second, the set of small tin compounds compiled by Bagno *et al.* is studied.[27] Structures are taken from ref. 57 and the BP86 functional[105,106] is applied with very large grids (grid size 5a).[110–112] Here, the x2c-TZVPPall-2c orbital and auxiliary basis sets[116] for the resolution of the identity approximation of the Coulomb integrals[117–120] (RI-*J*) are employed. SCF thresholds of $10^{-9}\,E_h$ and 10^{-8} a.u. are chosen, while a CPKS criterion of 10^{-7} a.u. is applied. The conductor-like screening model[121,122] (COSMO) is used for charged systems with the default settings[123] to simulate the counter ions. Again, the 1c DLU-X2C and 2c mSNSO-DLU-X2C Hamiltonians are considered. To illustrate the impact of the density functional approximation (DFA),[124–126] the following 31 functionals are studied. Pure DFAs are represented by BP86,[105,106] PBE,[127] TPSS,[128] M06-L,[129] M11-L,[130] MN12-L,[131] MN15-L,[132] TM,[133] and r^{2}SCAN,[134,135] while BH&HLYP,[105,136,137] B3LYP,[105,136,138] PBE0,[127,139] TPSSh,[128,140] M06,[141] M06-2X,[141] MN15,[142] and r^{2}SCAN0,[134,135,143] serve as examples for global hybrid

DFAs. Range-separated hybrids used are CAM-B3LYP,[144] ωB97X-D,[145] ωB97M,[146] M11,[147] revM11,[148] and MN12-SX.[149] The performance of local hybrid DFAs[150,151] is illustrated with LH07t-SVWN,[152] LH12ct-SsirPW92,[153] LH14t-calPBE,[154] LH20t,[155] PSTS,[71,156] LHJ14,[157] LHJ-HFcal,[158] and TMHF.[158] Note that local hybrids use a seminumerical scheme for the simultaneous evaluation of exact and semilocal exchange.[71,159–161] For the DFT study, the x2c-QZVPPall (auxiliary) basis sets are applied.[162]

Third, the efficiency of the 1c DLU-X2C and the 2c mSNSO-DLU-X2C approach is assessed for the low-valent Sn phosphinidenide complex [({SIDipp}P)$_2$Sn] (SIDipp = 1,3-bis(2,6-di-isopropylphenyl)-imidazolidin-2-ylidene) of ref. 163. Here, the BP86[105,106] and B3LYP functionals[105,136,138] are considered to illustrate the computational costs for pure and hybrid DFAs. Large grids[110,112] (grid size 4a) are chosen and both analytical integrals as well as seminumerical integrals are used for the exact exchange.[161] The RI-J approximation is used throughout. One-component calculations employ the x2c-TZVPall (auxiliary) basis sets,[116] whereas the x2c-TZVPall-2c bases are employed for the 2c calculations.[116] SCF thresholds of $10^{-9}\,\mathrm{E_h}$ and 10^{-8} a.u. for the root mean square of the densities matrices are applied. The CPKS procedure is converged up to a threshold of 10^{-6} a.u. for the norm of the residuum. Structures were optimized for each DFA, see txt file of the Supporting Information. Thus, only the structures for r^{2}SCAN,[134,135] LHJ-HFcal,[158] and TMHF[158] including the D4 dispersion correction[164–166] as well as that for ωB97X-D[145] were optimized in this work. Weight derivatives are included for r^{2}SCAN,[134,135] LHJ-HFcal,[158] and TMHF.[158] Structures for the other DFAs were already available in the literature.[57,163] For comparison with the experimental finding,[163] the top performers of the previous study are used together with the seminumerical exchange approximation (snK) for the CPKS part (grid size -1).[161] COSMO is applied with the settings for benzene,[121,122] i.e. a permitivity of $\epsilon = 2.300$ and a refractive index of $n = 1.4957$ are assumed.

Fourth, the $^1J(^{119}\mathrm{Sn},^{117}\mathrm{Sn})$ coupling constant of the novel pincer-type bis-stannylene ligand **SnNSn** is studied.[167] This compound features a very large through-space coupling

constant previously studied experimentally and computationally with the two-component mSNSO-DLU-X2C ansatz.[167] Here, the results are complemented with the SR X2C and the non-relativistic approach. For the first, the x2c-TZVPall (auxiliary) basis sets[116] are applied. For the latter, the def2-TZVP basis set[168] is used for all atoms except Sn, for which the TZVPall bases are used.[169] SCF convergence thresholds of $10^{-7}\,E_h$ and 10^{-6} a.u. for the root mean square of the densities matrices are chosen, while 10^{-7} a.u. is used for the norm of the CPKS residuum. Computational studies are carried out with the BH&HLYP,[105,136,137] PBE0,[127,139] TPSSh,[128,140] ωB97X-D,[145] and TMHF[158] functionals using large grids (grid size 3a).[110–112] Structures are taken from ref. 167. All calculations use the multipole-accelerated RI-J (MARI-J) approximation[170] and snK for the CPKS part. (grid size -1).[161]

4 Assessment of Accuracy and Efficiency

4.1 Tetrel Hydrogen Molecules

Comparison of the $^1J_{\mathrm{TtH}}$ coupling constant in Table 1 reveals pronounced relativistic effects for the heavy elements. Starting with GeH_4 the non-relativistic treatment is no longer sufficient. X2C and the 4c approach lead to a remarkable agreement for all molecules except PbH_4, which can be (at least partly) attributed to the different nuclear models for the vector potential. X2C employs the finite nucleus model, while the 4c ansatz uses the point-charge limit.[171] This deviation is, however, small compared to the impact of relativistic effects (column: NR–4c MAPD).

The 1c and 2c approaches lead to an excellent agreement up to SnH_4, as the mean absolute percent-wise deviation (MAPD) is below 5% (column: 1c–2c MAPD). As expected, the deviation increases with the atomic number of the tetrel atom. In all cases, the coupling constant is dominated by the Fermi-contact interaction (see Supporting Information) and the coupling between the FC, SD, and PSO terms is rather small for the isotropic constant. The second-order or DSO interaction is of almost no importance for the $^1J_{\mathrm{TtH}}$ coupling.

Table 1: Comparison of non-relativistic and relativistic approaches. 4c-RMB results are taken from ref. 39. Coupling constants ($^1J_{\mathrm{TtH}}$, $^2J_{\mathrm{HH}}$) are given in Hz. Experimental findings[172–175] (Expt.) were collected in ref. 39. Uncontracted Dyall-VTZ/pcJ-2 basis sets and the BP86 functional are employed. MAPD is the mean absolute percent-wise deviation and NR means non-relativistic. SR and SO refer to scalar and spin–orbit treatments, i.e. 1c and 2c approaches. MAPD is not computed for coupling constants below 1 Hz. Contributions of the individual terms are found in the Supporting Information. There, results with a pseudo-2c treatment for the DSO term are also shown.

	NR	SR X2C	SO X2C	4c RMB	Expt.	SR–SO MAPD	NR–4c MAPD
				$^1J_{\mathrm{TtH}}$			
CH_4	121.5	122.1	121.9	122.0	120.1	0.2	0.4
SiH_4	−195.1	−198.9	−198.6	−201.6	−201.1	0.1	3.2
GeH_4	−82.3	−91.2	−90.5	−90.4	−97.6	0.8	8.9
SnH_4	−1365.9	−1776.2	−1740.2	−1742.2	−1933.3	2.1	21.6
PbH_4	1269.3	2650.4	2511.3	2345.3	–	5.5	45.9
				$^2J_{\mathrm{HH}}$			
CH_4	−12.90	−10.35	−13.15	−13.50	−12.40	21.3	4.5
SiH_4	−0.82	1.18	−0.44	−0.56	2.75	–	–
GeH_4	5.28	11.01	7.81	7.79	7.69	41.0	32.3
SnH_4	6.99	17.50	14.55	14.30	15.30	20.2	51.1
PbH_4	7.23	41.38	36.66	30.87	–	12.9	76.6

Thus, the lack of the FC and SD integrals for the second-order derivative in the 1c ansatz is well legitimated by the reduction in computational costs.

In contrast, the $^2J_{\mathrm{HH}}$ couplings reveal a different picture, as the DSO and PSO terms are sizable. Still, the Fermi-contact interaction is the leading term. Using the PSO integrals only for the DSO term in the 1c ansatz leads to notably larger error as observed for $^1J_{\mathrm{TtH}}$. The trend of the $^2J_{\mathrm{HH}}$ coupling constant is still well described by all approaches. The larger deviation towards the 2c approach can be addressed to the second-order X2C response equations in RKB. Both the spin-independent and the spin-dependent first-order integral derivatives lead to sizable contributions. However, their simultaneous treatment is not possible in a strict one-component approach.

Improving the DSO term is possible by transforming the 1c density matrix to the 2c picture without SCF iterations, see Supporting Information (DSO p2c). Then, the DSO

integrals can be evaluated in the 2c fashion using complex algebra. The computational demands are still drastically reduced, as no 2c SCF procedure is required and the first-order terms are still computed in the 1c formalism. Alternatively, the RMB condition could be employed. Then, non-vanishing second-order integral derivatives for the spin-independent part of $\mathbf{\Pi}$ are found, see eq. (31) in ref. 56. However, the second-order integral derivatives of $\mathbf{W}$ are problematic in one-electron X2C.[56]

Taking together, the one-component ansatz yields encouraging results for coupling constants. Especially, coupling constants, which are not substantially affected by the DSO integrals, are calculated in excellent agreement with the self-consistent spin–orbit formalism.

4.2 Small Tin Compounds

The accuracy of the SR X2C approach is assessed in more detail in Table 2 for 19 molecules and 44 Sn coupling constants. For molecules not including halogen atoms, very small MAPDs, typically below 5%, are obtained. SnH_3^- is an exception in this regard. The MAPDs increase with the atomic number of the halogen atoms. For instance, it rises from 7.3% for $SnCl_4$ to 41.0% and 391.5% for $SnBr_4$ and SnI_4, respectively. Therefore, the complex SO X2C ansatz is needed for such systems. Similar findings hold for Me_3SnCl, Me_3SnBr, Me_3SnI (Me = CH_3) as well as the series Me_3SnBr, Me_2SnBr_2, $MeSnBr_3$. Overall, the subset consisting of $SnMe_4$, $(Me_3Sn)_2$, SnH_4, SnH_3^+, SnH_3^-, Me_3SnCl, Me_2SnCl_2, $MeSnCl_3$, $SnCl_4$, Me_3SnBr, and Me_2SnBr_2 can be studied rather accurately with the SR X2C ansatz, as all MAPDs are below 20%.

Notably, neither SR X2C nor SO X2C result in a reasonable agreement with the experimental findings. Changing the basis set from a triple-ζ to a quadruple-ζ basis set does not substantially improve the results, see Supporting Information. Therefore, more sophisticated density functional approximations are considered herein—especially functionals based on the kinetic energy density to identify different iso-orbital regions. Note that the kinetic energy density τ requires a generalization for magnetic properties.[182–184] Therefore, the paramag-

Table 2: Sn coupling constants in Hz for a set of small tin compounds compiled in ref. 27. Experimental findings[176–181] (Expt.) were collected in ref. 27. See this reference for details. MAPD denotes the mean absolute percent-wise deviation of the SR X2C approach vs. the SO X2C ansatz (BP86/x2c-TZVPall-2c).

			SR X2C				SO X2C			MAPD	Expt.
Molecule	^nJ	J(Sn,X)	FC+SD	PSO	DSO	Total	FC+SD+PSO	DSO	Total		
$SnMe_4$	1	C	−157.8	13.4	0.0	−144.5	−140.5	−0.1	−140.6	2.8	−340
	2	H	24.7	1.8	0.0	26.5	24.9	0.2	25.1	5.7	53.9
$(Me_3Sn)_2$	1	Sn	955.3	−36.5	0.0	918.8	869.3	0.1	869.5	5.7	4460
	1	C	−67.1	12.8	0.0	−54.4	−50.3	−0.1	−50.5	7.7	−240
	2	H	17.9	1.9	0.0	19.8	18.1	0.0	18.1	9.3	49
	2	C	−44.9	0.4	0.0	−44.5	−43.9	−0.1	−44.1	1.0	−56
	3	H	−17.0	0.0	0.1	−17.0	−16.9	0.0	−16.9	0.8	−17.3
SnH_4	1	H	−1532.1	3.7	0.0	−1528.4	−1496.5	0.0	−1496.5	2.1	−1930
SnH_3^+	1	H	−2101.9	17.5	0.0	−2084.4	−2012.5	0.1	−2012.4	3.6	−2960
SnH_3^-	1	H	159.4	−2.8	0.0	156.6	191.4	0.0	191.4	18.2	109.4
Me_3SnCl	1	Cl	260.0	46.4	0.0	306.4	290.9	0.0	290.9	5.3	220
	1	C	−170.5	19.0	0.0	−151.6	−146.8	−0.1	−146.9	3.2	−379.7
	2	H	23.6	2.3	0.0	26.0	24.2	0.1	24.3	6.9	58.2
Me_2SnCl_2	1	Cl	319.2	76.1	0.0	395.3	376.0	0.0	376.0	5.1	220
	1	C	−228.5	21.8	0.0	−206.7	−201.5	−0.1	−201.7	2.5	−468.4, −566
	2	H	27.7	2.3	0.0	30.1	28.3	0.1	28.3	6.1	68.2, 68.9
$MeSnCl_3$	1	Cl	395.4	90.5	0.0	485.9	460.3	0.0	460.3	5.6	–
	1	C	−392.6	20.9	−0.1	−371.7	−365.8	−0.1	−365.9	1.6	–
	2	H	45.6	2.1	0.0	47.6	46.0	0.0	46.0	3.5	96.9
$SnCl_4$	1	Cl	461.9	88.8	0.0	550.7	513.3	0.0	513.3	7.3	470
Me_3SnBr	1	Br	1373.5	217.6	0.0	1591.1	1384.2	−0.1	1384.1	14.9	–
	1	C	−157.2	19.2	0.0	−138.1	−134.2	−0.1	−134.4	2.8	−368.9, −380
	2	H	22.7	2.4	0.0	25.1	23.3	0.0	23.4	7.3	57.8
Me_2SnBr_2	1	Br	1691.6	378.6	0.0	2070.2	1765.3	−0.1	1765.2	17.3	–
	1	C	−192.1	22.2	−0.1	−170.0	−165.7	−0.2	−165.8	2.5	−442.7
	2	H	24.6	2.4	0.0	27.0	25.0	−0.1	24.9	8.4	66.7
$MeSnBr_3$	1	Br	2134.9	458.9	0.0	2593.8	2092.5	−0.1	2092.3	24.0	–
	1	C	−307.9	21.9	−0.1	−286.1	−277.9	−0.2	−278.1	2.9	−640
	2	H	37.4	2.1	−0.1	39.5	36.9	−0.2	36.7	7.5	–
$SnBr_4$	1	Br	2672.7	454.4	−0.1	3127.0	2217.8	−0.2	2217.6	41.0	920
Me_3SnI	1	I	1645.8	235.5	0.0	1881.3	1371.9	0.0	1371.9	37.1	–
	1	C	−142.2	18.9	−0.1	−123.4	−119.3	−0.1	−119.5	3.3	–
	2	H	21.8	2.5	0.0	24.2	22.6	0.0	22.6	7.3	–
Me_2SnI_2	1	I	1944.4	420.8	0.0	2365.2	1548.7	−0.1	1548.7	52.7	–
	1	C	−150.3	22.1	−0.1	−128.3	−118.0	−0.2	−118.2	8.5	–
	2	H	20.7	2.7	−0.1	23.3	20.9	−0.2	20.7	12.5	–
$MeSnI_3$	1	I	2256.2	520.1	0.0	2776.3	1376.3	−0.1	1376.1	101.7	–
	1	C	−214.7	22.8	−0.1	−192.0	−155.8	−0.2	−156.0	23.0	–
	2	H	25.4	2.6	−0.1	27.9	22.3	−0.3	22.0	26.8	–
SnI_4	1	I	2578.3	527.0	0.0	3105.2	632.0	−0.1	631.8	391.5	940
$SnCl_3I$	1	Cl	430.7	89.8	0.0	520.4	468.6	−0.1	468.6	11.1	378
	1	I	4135.7	518.3	0.0	4654.0	2138.1	−0.1	2138.0	117.7	1638
SnI_3Cl	1	Cl	364.5	92.1	0.0	456.6	386.6	−0.1	386.5	18.2	421
	1	I	3034.8	523.4	0.0	3558.2	1050.2	−0.1	1050.1	238.9	1097

netic current density and the magnetic kernel are included for the PSO term.[58,71] This means that an iterative procedure is necessary for this term. However, the impact on the computational costs is rather small, as the FC+SD part is unaffected and involves nine response equations per nucleus, while only three equations are to be solved for the PSO contribu-

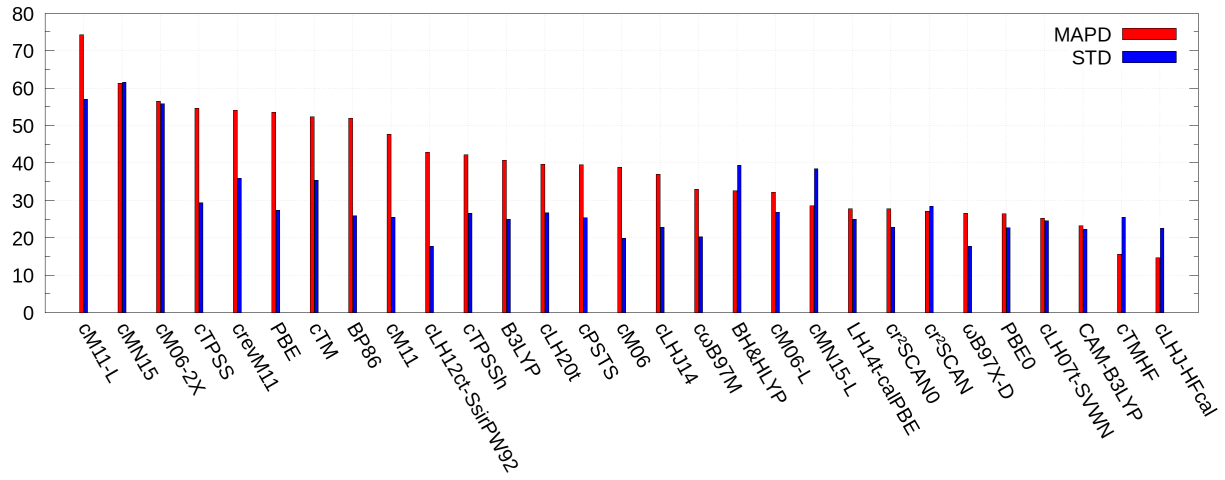

Figure 1: Comparison of various density functional approximations (SR X2C/x2c-QZVPPall) to the experimental findings[176–181] of selected Sn compounds. A "c" at the beginning of the acronym indicates that the response of the current density is included for the PSO term. MAPD and STD denote the mean absolute percent-wise deviation and its standard deviation. Complete data is available in the Supporting Information.

tion. For the 1c ansatz, the current density does not affect the ground-state calculation—in contrast to the 2c treatment.[185]

The results are shown in Figure 1, see Supporting Information for complete data. Generally, pure density functionals do not yield accurate results and hybrid functionals are clearly superior. Notable exceptions in this regard are r^{2}SCAN, M06-L, and MN15-L which perform on par with the best global hybrid functionals (BH&HLYP, r^{2}SCAN0, PBE0). For r^{2}SCAN, adding exact exchange even leads to a minor deterioration. Range-separated and local hybrid functionals allow for a more sophisticated and flexible admixture of exact exchange and tend to improve the accuracy. This is illustrated by the fact that the four top performers are LH07t-SVWN, CAM-B3LYP, TMHF, and LHJ-HFcal. Only TMHF and LHJ-HFcal yield MAPDs below 20%. The respective errors amount to 15.6% and 14.7%, which is in good agreement with all experimental findings. This shows that local hybrids are about to become an increasingly useful class of density functional approximations.

Overall, the SR X2C ansatz accurately describes the Sn coupling constants for organometallic compounds excluding heavy halogen atoms. The error by not treating spin–orbit coupling

self-consistently is minuscule compared to the impact of different density functional approximations. Local hybrids tend to perform best for the Sn coupling constants, with TMHF and LHJ-HFcal leading to the smallest deviation from experiment. Additionally, r^{2}SCAN shows very promising results.

4.3 Tin–Phosphorous Coupling

Third, the efficiency is assessed. To do so, the wall times for the SCF and NMR coupling calculation of [({SIDipp}P)$_2$Sn] on an Intel Xeon Gold 6212U CPU (2.40 GHz) using 12 OpenMP threads are listed in Table 3. For the 1c approach, the SCF and NMR calculation almost take the same computation time, BP86 requires 9 minutes for the SCF and 6 minutes for the NMR calculation. For B3LYP, the computation times amount to 114 minutes and 116 minutes, respectively. This means that, in terms of computational costs, the NMR calculation can always be carried out if the SCF procedure is affordable. This is not true for the 2c calculations. Here, the exchange integrals for the CPKS equations are very demanding. For B3LYP, the SCF part amounts to 591 minutes, while the CPKS part takes 2709 minutes. Thus, the NMR calculation is more involved than the SCF procedure. Overall, the 1c approach leads to a speed-up by factors of 10 (SCF) and 8 (SSCCs) for BP86, and to an acceleration of 5 and 23 with B3LYP. The results are only slightly affected, e.g., the Sn–P coupling constant changes by 5 Hz from 1388 to 1383 Hz. The two Sn–P couplings were averaged for comparison with the experiment.[163] The computed couplings differ by 1–5 Hz.

Analyzing the NMR computation in more detail, it becomes evident that the time for the one-electron part is negligible and large-scale calculations are routinely possible, i.e. DLU substantially reduces the computation time without introducing notable errors.[57,78,98,104,186–190] The wall times are always dominated by the HF or exact exchange integrals—just like in the standard non-relativistic framework.[66] Therefore, established approximations such as the resolution of the identity approximation to the exchange integrals[191] (RI-K) or the seminumerical exchange approximation[159,161,192–199] are pivotal. Application of the seminumerical

Table 3: Wall times and iterations (Iter.) for the SCF procedure and the main steps of the calculation of the two Sn–P spin–spin coupling constants (SSCCs) of [({SIDipp}P)$_2$Sn] on an Intel Xeon Gold 6212U CPU (2.40 GHz) using 12 OpenMP threads. Code was compiled with Intel Fortran Compiler 19.0.1.144. Timings are listed in minutes. The extended Hückel method is used for the SCF initial guess. The RI-J approximation is employed for the SCF procedure and the seminumerical exchange approximation (snK) is applied in the CPKS part if stated explicitly. CPKS iterations are given for both the FC+SD (first number) and the PSO parts (second number) in 1c runs. Zero iterations for the PSO term indicates that no iterations and no evaluation of the two-electron integrals in the CPKS part were needed.

	SCF		SSCCs				
Method	Iter.	Total Time	Iter.	1e Part	HF Exchange	XC Kernel	Total Time
1c BP86	26	9	6,0	1	–	5	6
2c BP86	88	88	6	4	–	43	50
1c B3LYP	26	114	7,5	1	106	6	116
2c B3LYP	115	591	8	4	2650	49	2709
1c B3LYP snK	–	–	7,5	1	25	6	31
2c B3LYP snK	–	–	10	4	223	79	323

exchange approximation to the CPKS part, reduces the wall times for B3LYP substantially, while changing the results by 1–2 Hz only, see also ref. 57. The 1c and 2c calculations now take 31 and 323 minutes. Especially for the 2c formalism, a drastic speed-up is found. This makes scalar and spin–orbit calculations computationally affordable using low-cost hardware.

Results for the Sn–P coupling constant are listed in Table 4 with selected top performers of the previous study in Section 4.2. Here, the conductor-like screening model is included for a better comparison with the experiment in solution. Timings above were measured without COSMO. According to the results in Table 4, the DSO term is negligible, which is also confirmed by the 2c calculations.[57] In contrast to the Sn compounds of Table 2, the PSO term is of great importance for the total coupling constant. It amounts to almost a third of the $^1J(^{119}\mathrm{Sn},^{31}\mathrm{P})$ constant and the remaining two thirds may be attributed to the FC+SD term. All functionals result in a fairly good agreement with the experiment. BP86 overestimates the coupling constant by about 4% and the conventional global and range-separated hybrid functionals further increase the coupling constant. Therefore, they lead to a larger deviation. Especially CAM-B3LYP notably increases the results compared to

Table 4: Mean $^{1}J(^{119}\mathrm{Sn},^{31}\mathrm{P})$ spin–spin coupling constant (in Hz) of [({SIDipp}P)$_2$Sn] with various density functional approximations and the x2c-TZVPall basis sets. Experimental result (Expt.) taken from ref. 163. A "c" at the beginning of the acronym indicates that the response of the current density is included for the PSO term. QZVPP refers to the x2c-QZVPPall basis set, which employs more than 5838 functions (spherical AO basis).

Method	FC+SD	PSO	DSO	Total J
BP86	892	503	−0.1	1394
r^{2}SCAN	989	421	−0.1	1410
cr^{2}SCAN	989	441	−0.1	1430
B3LYP	913	527	−0.1	1440
PBE0	936	478	−0.1	1413
CAM-B3LYP	1016	551	−0.1	1567
ωB97X-D	941	508	−0.1	1450
cLHJ-HFcal	980	469	−0.1	1449
cTMHF	941	464	−0.1	1405
BP86 QZVPP	981	507	−0.1	1488
B3LYP QZVPP	1045	533	−0.1	1578
Expt.	–	–	–	1334

B3LYP and BP86. The local hybrids TMHF and LHJ-HFcal lead to coupling constants of 1405 Hz and 1449 Hz.

In short, a relativistic one-component approach drastically reduces the wall times for large systems and allows for routine studies with modern density functional methods.

4.4 Tin Pincer Ligand and Sn–Sn Coupling Constant

The novel pincer-type bis-stannylene ligand **SnNSn**, depicted in Figure 2, recently allowed us to synthesize and study coinage metal complexes with Cu(I), Ag(I), and Au(I).[167] Here, the coinage metals are stabilized in exclusively tetrahedral coordination geometries. The pincer ligand itself shows a very large $^{1}J(^{119}\mathrm{Sn},^{117}\mathrm{Sn})$ coupling constant of 4087 Hz. However, the electron density between the two Sn atoms indicates no notable covalent bonding interaction. The self-consistent SO X2C approach resulted in a good agreement with the experimental findings.[167] Herein, SO X2C results are compared to the SR X2C approach and the non-relativistic treatment as shown in Table 5.

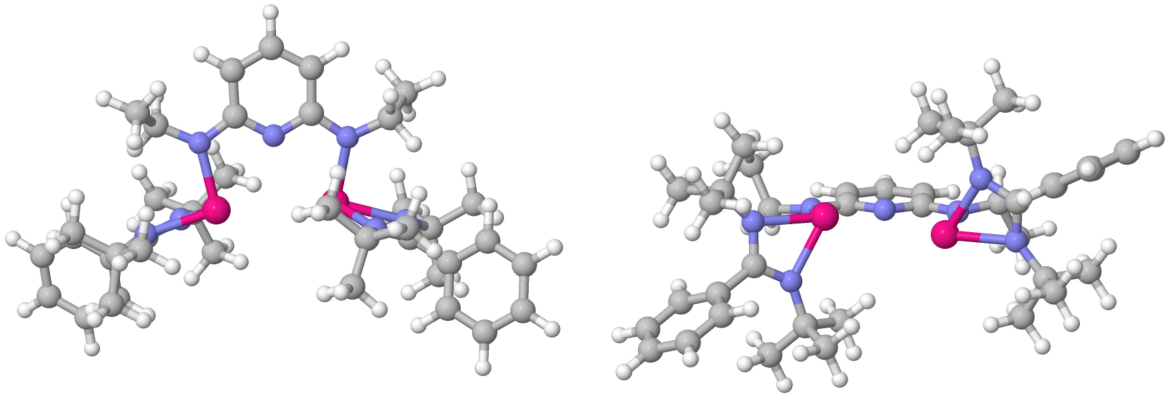

Figure 2: Molecular structure of the pincer-type bis-stannylene ligand **SnNSn**. The compound consists of 107 atoms and was synthesized in ref. 167. Color code: H white, C grey, N purple, and Sn pink. Left: top-view, right: side-view.

Table 5: $^{1}J(^{119}\mathrm{Sn},^{117}\mathrm{Sn})$ coupling constant in Hz of a novel pincer-type bis-stannylene ligand **SnNSn**. NR, SR X2C, and SO X2C denote the non-relativistic, scalar X2C, and spin–orbit X2C approach, respectively. A "c" at the beginning of the DFA acronym indicates that the response of the current density is included for the PSO term. Two-component (x2c-TZVPall-2c basis) and experimental results taken from ref. 167. Non-relativistic (TZVPall/def2-TZVP basis) and scalar X2C (x2c-TZVPall basis) calculations are carried out herein. Computation times are listed in the Supporting Information.

Functional	NR	SR X2C	SO X2C
BH&HLYP	2358.8	5504.3	5499.5
PBE0	1947.8	4806.0	4802.1
cTPSSh	2065.3	4782.8	4768.2
ωB97X-D	3092.6	6545.2	6538.6
cTMHF	2203.1	5147.9	5135.8
Expt.		4087	

The non-relativistic formalism is clearly insufficient, as it underestimates the coupling constant by more than 50%. In contrast, the SR X2C and SO X2C lead to practically the same results, which are generally in better agreement with the experimental findings. As shown by the computation times in the Supporting Information, the computational demands of the non-relativistic and the SR X2C approach are very similar with the all-electron basis sets used herein. Note that relativistic basis sets are somewhat larger. Therefore, the SR X2C ansatz can be safely applied to this Sn compound, which confirms the findings of Section 4.2.

Considering the functionals, PBE0, cTPSSh, and TMHF lead to a deviation of about 25% towards the experiment, whereas ωB97X-D severely overestimates the coupling constant by around 60%. BH&HLYP represents an intermediate case with a deviation of 34% towards the experimental result. Individual contributions of the terms are listed in the Supporting Information. Accordingly, the total coupling constant is completely dominated by the FC+SD term, making up almost 100% of the total coupling constant.

Overall, this shows that the one-component approach presented herein can be accurately applied to large and "real-world" organometallic compounds including heavy elements.

5 Summary and Conclusion

This work presents a low-cost scalar X2C ansatz for NMR coupling constant, which drastically reduces the computational demands of the self-consistent spin–orbit approach presented previously.[56,57] The errors introduced by truncating the complex two-component approach to a one-component ansatz, which does not make use of complex algebra, is critically assessed. For instance, the accuracy deteriorates with the number and mass of the halogen atoms in a molecule, as this leads to more and more pronounced spin–orbit effects. Furthermore, notable errors are found for coupling constants driven by the unperturbed density contribution, which corresponds to the diamagnetic spin–orbit term. For many coupling constants, this term is the smallest contribution and therefore the errors seem justified by the reduced computational demands. A straightforward strategy to overcome this limitation is discussed.

The approach outlined herein is also intended for the development of NMR-tailored basis sets, as basis set optimization typically requires a large test set including all elements of interest[109,112,116,162,168,200–208] and many iterations until convergence is reached with respect to the optimized exponents and contraction coefficients for all systems. Such developments of basis sets for NMR coupling constants will be the topic of future work.

Given that the number of quantum chemical program suites supporting a scalar X2C

or exact one-component (X1C) treatment is far larger than the number of program suites featuring a two-component formalism (see, e.g., ref. 209), the ansatz presented herein may also help to make modern relativistic all-electron approaches available in many program and thus make it available to the masses.

Acknowledgement

I thank Sebastian Gillhuber, Christof Holzer, Fabian Mack, and Florian Weigend for discussions. Furthermore, I am grateful to Georgi L. Stoychev for discussions on X2C and magnetic properties. I thank Matthias Haasler and Martin Kaupp for sharing the D4 parameters of TMHF and LHJ-HFcal. I acknowledge financial support by Turbomole GmbH. Most routines were developed while I was supported through a fellowship by Fonds der Chemischen Industrie (FCI, German Chemical Industry Funds). This work used computer hardware funded by FCI.

Supporting Information Available

The Supporting Information is available

- Contribution of terms to the couplings of TtH_4 (PDF)
- Individual results for statistical evaluation of the Sn couplings (PDF)
- Computation times for the pincer-type ligand **SnNSn** (PDF)
- Contribution of the coupling terms for **SnNSn** (PDF)
- All structures employed in the studies of this work (txt)

Data Availability Statement

The data that support the findings of this study are available within the article and its supplementary material.

References

(1) Mason, J., Ed. *Multinuclear NMR*; Springer US: New York, USA, 1987.

(2) Friebolin, H. *Basic One- and Two-Dimensional NMR Spectroscopy*, 5th ed.; Wiley-VCH: Weinheim, Germany, 2010.

(3) Wüthrich, K. NMR Studies of Structure and Function of Biological Macromolecules (Nobel Lecture). *Angew. Chem. Int. Ed.* **2003**, *42*, 3340–3363.

(4) Helgaker, T.; Jaszuński, M.; Ruud, K. Ab initio methods for the calculation of NMR shielding and indirect spin-spin coupling constants. *Chem Rev.* **1999**, *99*, 293–352.

(5) Vaara, J. Theory and computation of nuclear magnetic resonance parameters. *Phys. Chem. Chem. Phys.* **2007**, *9*, 5399–5148.

(6) Helgaker, T.; Jaszuński, M.; Pecul, M. The quantum-chemical calculation of NMR indirect spin–spin coupling constants. *Prog. Nucl. Magn. Reson. Spectrosc.* **2008**, *53*, 249–268.

(7) Kaupp, M., Bühl, M., Malkin, V. G., Eds. *Calculation of NMR and EPR Parameters: Theory and Applications*; Wiley-VCH: Weinheim, Germany, 2004.

(8) Dyall, K. G.; Fægri Jr., K. *Introduction to Relativistic Quantum Chemistry*; Oxford University Press: New York, USA, 2007.

(9) Reiher, M.; Wolf., A. *Relativistic Quantum Chemistry – The Fundamental Theory of Molecular Science*, 2nd ed.; Wiley-VCH: Weinheim, Germany, 2015.

(10) Liu, W., Ed. *Handbook of Relativistic Quantum Chemistry*; Springer: Berlin, Heidelberg, Germany, 2017.

(11) Pyykkö, P. Relativistic Effects in Chemistry: More Common Than You Thought. *Annu. Rev. Phys. Chem.* **2012**, *63*, 45.

(12) Autschbach, J. Perspective: Relativistic effects. *J. Chem. Phys.* **2012**, *136*, 150902.

(13) Repisky, M.; Komorovsky, S.; Bast, R.; Ruud, K. Relativistic Calculations of Nuclear Magnetic Resonance Parameters. In *Gas Phase NMR*; Jackowski, K., Jaszuński, M., Eds.; The Royal Society of Chemistry: Cambridge, United Kingdom, 2016; Chapter 8, pp 267–303.

(14) Liu, W. Big picture of relativistic molecular quantum mechanics. *Natl. Sci. Rev.* **2016**, *3*, 204–221.

(15) Liu, W. Essentials of relativistic quantum chemistry. *J. Chem. Phys.* **2020**, *152*, 180901.

(16) Dolg, M.; Cao, X. Relativistic Pseudopotentials: Their Development and Scope of Applications. *Chem. Rev.* **2012**, *112*, 403–480.

(17) Saue, T. Relativistic Hamiltonians for Chemistry: A Primer. *ChemPhysChem* **2011**, *12*, 3077–3094.

(18) Liu, W. Ideas of relativistic quantum chemistry. *Mol. Phys.* **2010**, *108*, 1679–1706.

(19) Cheng, L.; Stopkowicz, S.; Gauss, J. Analytic energy derivatives in relativistic quantum chemistry. *Int. J. Quantum Chem.* **2014**, *114*, 1108–1127.

(20) Peng, D.; Reiher, M. Exact decoupling of the relativistic Fock operator. *Theor. Chem. Acc.* **2012**, *131*, 1081.

(21) Cremer, D.; Zou, W.; Filatov, M. Dirac-exact relativistic methods: the normalized elimination of the small component method. *Wiley Interdiscip. Rev.: Comput. Mol. Sci.* **2014**, *4*, 436–467.

(22) Aucar, G. A.; Melo, J. I.; Aucar, I. A.; Maldonado, A. F. Foundations of the LRESC model for response properties and some applications. *Int. J. Quantum Chem.* **2018**, *118*, e25487.

(23) Reiher, M. Douglas–Kroll–Hess Theory: a relativistic electrons-only theory for chemistry. *Theor. Chem. Acc.* **2006**, *116*, 241–252.

(24) Reiher, M. Relativistic Douglas-Kroll-Hess theory. *Wiley Interdiscip. Rev.: Comput. Mol. Sci.* **2012**, *2*, 139–149.

(25) Nakajima, T.; Hirao, K. The Douglas–Kroll–Hess Approach. *Chem. Rev.* **2012**, *112*, 385–402.

(26) Nakanishi, W.; Hayashi, S.; Katsura, Y.; Hada, M. Relativistic Effect on ^{77}Se NMR Chemical Shifts of Various Selenium Species in the Framework of Zeroth-Order Regular Approximation. *J. Phys. Chem. A* **2011**, *115*, 8721–8730.

(27) Bagno, A.; Casella, G.; Saielli, G. Relativistic DFT Calculation of ^{119}Sn Chemical Shifts and Coupling Constants in Tin Compounds. *J. Chem. Theory Comput.* **2006**, *2*, 37–46.

(28) Moncho, S.; Autschbach, J. Relativistic Zeroth-Order Regular Approximation Combined with Nonhybrid and Hybrid Density Functional Theory: Performance for NMR Indirect Nuclear Spin–Spin Coupling in Heavy Metal Compounds. *J. Chem. Theory Comput.* **2010**, *6*, 223–234.

(29) Autschbach, J. Relativistic calculations of magnetic resonance parameters: back-

ground and some recent developments. *Philos. Trans. Royal Soc. A* **2014**, *372*, 20120489.

(30) Ruud, K.; Demissie, T. B.; Jaszuński, M. Ab initio and relativistic DFT study of spin–rotation and NMR shielding constants in XF_6 molecules, X = S, Se, Te, Mo, and W. *J. Phys. Chem.* **2014**, *140*, 194308.

(31) Maldonado, A. F.; Aucar, G. A. Relativistic and Electron-Correlation Effects on the Nuclear Magnetic Resonance Shieldings of Molecules Containing Tin and Lead Atoms. *J. Phys. Chem. A* **2014**, *118*, 7863–7875.

(32) Demissie, T. B.; Kostenko, N.; Komorovsky, S.; Repisky, M.; Isaksson, J.; Bayer, A.; Ruud, K. Experimental and four-component relativistic DFT studies of tungsten carbonyl complexes. *J. Phys. Org. Chem.* **2015**, *28*, 723–731.

(33) Giménez, C. A.; Maldonado, A. F.; Aucar, G. A. Relativistic and electron correlation effects on NMR J-coupling of Sn and Pb containing molecules. *Theor. Chem. Acc.* **2016**, *135*, 201.

(34) Demissie, T. B. Relativistic effects on the NMR parameters of Si, Ge, Sn, and Pb alkynyl compounds: Scalar versus spin-orbit effects. *J. Chem. Phys.* **2017**, *147*, 174301.

(35) Stückrath, J. B.; Gasevic, T.; Bursch, M.; Grimme, S. Benchmark Study on the Calculation of ^{119}Sn NMR Chemical Shifts. *Inorg. Chem.* **2022**, *61*, 3903–3917.

(36) Enevoldsen, T.; Visscher, L.; Saue, T.; Jensen, H. J. A.; Oddershede, J. Relativistic four-component calculations of indirect nuclear spin–spin couplings in MH_4 (M=C, Si, Ge, Sn, Pb) and $Pb(CH_3)_3H$. *J. Chem. Phys.* **2000**, *112*, 3493–3498.

(37) Visscher, L.; Enevoldsen, T.; Saue, T.; Jensen, H. J. A.; Oddershede, J. Full four-

component relativistic calculations of NMR shielding and indirect spin–spin coupling tensors in hydrogen halides. *J. Comput. Chem.* **1999**, *20*, 1262–1273.

(38) Gomez, S. S.; Romero, R. H.; Aucar, G. A. Fully relativistic calculation of nuclear magnetic shieldings and indirect nuclear spin-spin couplings in group-15 and -16 hydrides. *J. Chem. Phys.* **2002**, *117*, 7942–7946.

(39) Repiský, M.; Komorovský, S.; Malkina, O. L.; Malkin, V. G. Restricted magnetically balanced basis applied for relativistic calculations of indirect nuclear spin–spin coupling tensors in the matrix Dirac–Kohn–Sham framework. *Chem. Phys.* **2009**, *356*, 236–242.

(40) Foldy, L. L.; Wouthuysen, S. A. On the Dirac Theory of Spin 1/2 Particles and Its Non-Relativistic Limit. *Phys. Rev.* **1950**, *78*, 29–36.

(41) Heully, J.-L.; Lindgren, I.; Lindroth, E.; Lundqvist, S.; Mårtensson-Pendrill, A.-M. Diagonalisation of the Dirac Hamiltonian as a basis for a relativistic many-body procedure. *J. Phys. B: At. Mol. Phys.* **1986**, *19*, 2799–2815.

(42) Chang, C.; Pelissier, M.; Durand, P. Regular Two-Component Pauli-Like Effective Hamiltonians in Dirac Theory. *Phys. Scr.* **1986**, *34*, 394–404.

(43) van Lenthe, E.; Baerends, E. J.; Snijders, J. G. Relativistic regular two-component Hamiltonians. *J. Phys. Chem.* **1993**, *99*, 4597–4610.

(44) van Lenthe, E.; Baerends, E. J.; Snijders, J. G. Relativistic total energy using regular approximations. *J. Chem. Phys.* **1994**, *101*, 9783–9792.

(45) Kutzelnigg, W.; Liu, W. Quasirelativistic theory equivalent to fully relativistic theory. *J. Chem. Phys.* **2005**, *123*, 241102.

(46) Liu, W.; Kutzelnigg, W. Quasirelativistic theory. II. Theory at matrix level. *J. Chem. Phys.* **2007**, *126*, 114107.

(47) Liu, W.; Peng, D. Infinite-order quasirelativistic density functional method based on the exact matrix quasirelativistic theory. *J. Chem. Phys.* **2006**, *125*, 044102.

(48) Liu, W.; Peng, D. Erratum: "Infinite-order quasirelativistic density functional method based on the exact matrix quasirelativistic theory" [J. Chem. Phys. 125, 044102 (2006)]. *J. Chem. Phys.* **2006**, *125*, 149901.

(49) Iliaš, M.; Saue, T. An infinite-order two-component relativistic Hamiltonian by a simple one-step transformation. *J. Chem. Phys.* **2007**, *126*, 064102.

(50) Liu, W.; Peng, D. Exact two-component Hamiltonians revisited. *J. Chem. Phys.* **2009**, *131*, 031104.

(51) Peng, D.; Liu, W.; Xiao, Y.; Cheng, L. Making four- and two-component relativistic density functional methods fully equivalent based on the idea of "from atoms to molecule". *J. Chem. Phys.* **2007**, *127*, 104106.

(52) Autschbach, J.; Ziegler, T. Nuclear spin–spin coupling constants from regular approximate relativistic density functional calculations. I. Formalism and scalar relativistic results for heavy metal compounds. *J. Chem. Phys.* **2000**, *113*, 936–947.

(53) Autschbach, J.; Ziegler, T. Nuclear spin–spin coupling constants from regular approximate relativistic density functional calculations. II. Spin–orbit coupling effects and anisotropies. *J. Chem. Phys.* **2000**, *113*, 9410–9418.

(54) Autschbach, J. Two-component relativistic hybrid density functional computations of nuclear spin-spin coupling tensors using Slater-type basis sets and density-fitting techniques. *J. Chem. Phys.* **2008**, *129*, 094105.

(55) Autschbach, J. Erratum: Two-component relativistic hybrid density functional computations of nuclear spin-spin coupling tensors using Slater-type basis sets and density-

fitting techniques [J. Chem. Phys. 129, 094105 (2008)]. *J. Chem. Phys.* **2009**, *130*, 209901.

(56) Yoshizawa, T. On the development of the exact two-component relativistic method for calculating indirect NMR spin-spin coupling constants. *Chem. Phys.* **2019**, *518*, 112–122.

(57) Franzke, Y. J.; Mack, F.; Weigend, F. NMR Indirect Spin–Spin Coupling Constants in a Modern Quasirelativistic Density Functional Framework. *J. Chem. Theory Comput.* **2021**, *17*, 3974–3994.

(58) Franzke, Y. J.; Holzer, C.; Mack, F. NMR Coupling Constants Based on the Bethe–Salpeter Equation in the *GW* Approximation. *J. Chem. Theory Comput.* **2022**, *18*, 1030–1045.

(59) Lide, D. R., Ed. *CRC Handbook of Chemistry and Physics*, 78th ed.; CRC Press: Boca Ratón, USA, 1997.

(60) Stone, N. Table of nuclear magnetic dipole and electric quadrupole moments. *At. Data Nucl. Data Tables* **2005**, *90*, 75–176.

(61) Ramsey, N. F. Electron Coupled Interactions between Nuclear Spins in Molecules. *Phys. Rev.* **1953**, *91*, 303–307.

(62) CODATA internationally recommened 2018 values of the fundamental physical constans, `https://physics.nist.gov/cuu/Constants/index.html` (retrieved December 28, 2020).

(63) Malkina, O. L.; Salahub, D. R.; Malkin, V. G. Nuclear magnetic resonance spin–spin coupling constants from density functional theory: Problems and results. *J. Chem. Phys.* **1996**, *105*, 8793–8800.

(64) Dickson, R. M.; Ziegler, T. NMR Spin–Spin Coupling Constants from Density Functional Theory with Slater-Type Basis Functions. *J. Phys. Chem.* **1996**, *100*, 5286–5290.

(65) Sychrovský, V.; Gräfenstein, J.; Cremer, D. Nuclear magnetic resonance spin–spin coupling constants from coupled perturbed density functional theory. *J. Chem. Phys.* **2000**, *113*, 3530–3547.

(66) Mack, F.; Schattenberg, C. J.; Kaupp, M.; Weigend, F. Nuclear Spin–Spin Couplings: Efficient Evaluation of Exact Exchange and Extension to Local Hybrid Functionals. *J. Phys. Chem. A* **2020**, *124*, 8529–8539.

(67) Casida, M. E. Time-dependent density-functional theory for molecules and molecular solids. *J. Mol. Struct.: THEOCHEM* **2009**, *914*, 3–18.

(68) Furche, F.; Krull, B. T.; Nguyen, B. D.; Kwon, J. Accelerating molecular property calculations with nonorthonormal Krylov space methods. *J. Chem. Phys.* **2016**, *144*, 174105.

(69) Bates, J. E.; Furche, F. Harnessing the meta-generalized gradient approximation for time-dependent density functional theory. *J. Chem. Phys.* **2012**, *137*, 164105.

(70) Bates, J. E.; Heiche, M. C.; Liang, J.; Furche, F. Erratum: "Harnessing the meta-generalized gradient approximation for time-dependent density functional theory" [J. Chem. Phys. 137, 164105 (2012)]. *J. Chem. Phys.* **2022**, *156*, 159902.

(71) Holzer, C.; Franzke, Y. J.; Kehry, M. Assessing the Accuracy of Local Hybrid Density Functional Approximations for Molecular Response Properties. *J. Chem. Theory Comput.* **2021**, *17*, 2928–2947.

(72) Stanton, R. E.; Havriliak, S. Kinetic balance: A partial solution to the problem of variational safety in Dirac calculations. *J. Chem. Phys.* **1984**, *81*, 1910–1918.

(73) Gell-Mann, M. The interpretation of the new particles as displaced charge multiplets. *Nuovo Cim.* **1956**, *4*, 848–866.

(74) Bohr, A.; Weisskopf, V. F. The Influence of Nuclear Structure on the Hyperfine Structure of Heavy Elements. *Phys. Rev.* **1950**, *77*, 94–98.

(75) Hennum, A. C.; Klopper, W.; Helgaker, T. Direct perturbation theory of magnetic properties and relativistic corrections for the point nuclear and Gaussian nuclear models. *J. Chem. Phys.* **2001**, *115*, 7356–7363.

(76) Malkin, E.; Malkin, I.; Malkina, O. L.; Malkin, V. G.; Kaupp, M. Scalar relativistic calculations of hyperfine coupling tensors using the Douglas–Kroll–Hess method with a finite-size nucleus model. *Phys. Chem. Chem. Phys.* **2006**, *8*, 4079–4085.

(77) Autschbach, J. Magnitude of Finite-Nucleus-Size Effects in Relativistic Density Functional Computations of Indirect NMR Nuclear Spin–Spin Coupling Constants. *ChemPhysChem* **2009**, *10*, 2274–2283.

(78) Franzke, Y. J.; Weigend, F. NMR Shielding Tensors and Chemical Shifts in Scalar-Relativistic Local Exact Two-Component Theory. *J. Chem. Theory Comput.* **2019**, *15*, 1028–1043.

(79) Dyall, K. G. Interfacing relativistic and nonrelativistic methods. I. Normalized elimination of the small component in the modified Dirac equation. *J. Chem. Phys.* **1997**, *106*, 9618–9626.

(80) Dyall, K. G. Interfacing relativistic and nonrelativistic methods. II. Investigation of a low-order approximation. *J. Chem. Phys.* **1998**, *109*, 4201–4208.

(81) Dyall, K. G.; Enevoldsen, T. Interfacing relativistic and nonrelativistic methods. III. Atomic 4-spinor expansions and integral approximations. *J. Chem. Phys.* **1999**, *111*, 10000–10007.

(82) Dyall, K. G. Interfacing relativistic and nonrelativistic methods. IV. One- and two-electron scalar approximations. *J. Chem. Phys.* **2001**, *115*, 9136–9143.

(83) Cheng, L.; Gauss, J. Analytic energy gradients for the spin-free exact two-component theory using an exact block diagonalization for the one-electron Dirac Hamiltonian. *J. Chem. Phys.* **2011**, *135*, 084114.

(84) Zou, W.; Filatov, M.; Cremer, D. Development and application of the analytical energy gradient for the normalized elimination of the small component method. *J. Chem. Phys.* **2011**, *134*, 244117.

(85) Cheng, L.; Gauss, J. Analytic second derivatives for the spin-free exact two-component theory. *J. Chem. Phys.* **2011**, *135*, 244104.

(86) Zou, W.; Filatov, M.; Cremer, D. Development, Implementation, and Application of an Analytic Second Derivative Formalism for the Normalized Elimination of the Small Component Method. *J. Chem. Theory Comput.* **2012**, *8*, 2617–2629.

(87) Kehry, M.; Franzke, Y. J.; Holzer, C.; Klopper, W. Quasirelativistic two-component core excitations and polarisabilities from a damped-response formulation of the Bethe–Salpeter equation. *Mol. Phys.* **2020**, *118*, e1755064.

(88) Dyall, K. G. An exact separation of the spin-free and spin-dependent terms of the Dirac–Coulomb–Breit Hamiltonian. *J. Chem. Phys.* **1994**, *100*, 2118–2127.

(89) Kutzelnigg, W. Origin and meaning of the Fermi contact interaction. *Theor. Chim. Acta* **1988**, *73*, 173–200.

(90) Autschbach, J. Relativistic Effects on Electron–Nucleus Hyperfine Coupling Studied with an Exact 2-Component (X2C) Hamiltonian. *J. Chem. Theory Comput.* **2017**, *13*, 710–718.

(91) Feng, R.; Duignan, T. J.; Autschbach, J. Electron–Nucleus Hyperfine Coupling Calculated from Restricted Active Space Wavefunctions and an Exact Two-Component Hamiltonian. *J. Chem. Theory Comput.* **2021**, *17*, 255–268.

(92) Gillhuber, S.; Franzke, Y. J.; Weigend, F. Paramagnetic NMR Shielding Tensors and Ring Currents: Efficient Implementation and Application to Heavy Element Compounds. *J. Phys. Chem. A* **2021**, *125*, 9707–9723.

(93) Bruder, F.; Franzke, Y. J.; Weigend, F. Paramagnetic NMR Shielding Tensors Based on Scalar Exact Two-Component and Spin–Orbit Perturbation Theory. *J. Phys. Chem. A* **2022**, *126*, 5050–5069.

(94) Ahlrichs, R.; Bär, M.; Häser, M.; Horn, H.; Kölmel, C. Electronic structure calculations on workstation computers: The program system turbomole. *Chem. Phys. Lett.* **1989**, *162*, 165–169.

(95) Furche, F.; Ahlrichs, R.; Hättig, C.; Klopper, W.; Sierka, M.; Weigend, F. Turbomole. *Wiley Interdiscip. Rev.: Comput. Mol. Sci.* **2014**, *4*, 91–100.

(96) Balasubramani, S. G.; Chen, G. P.; Coriani, S.; Diedenhofen, M.; Frank, M. S.; Franzke, Y. J.; Furche, F.; Grotjahn, R.; Harding, M. E.; Hättig, C.; Hellweg, A.; Helmich-Paris, B.; Holzer, C.; Huniar, U.; Kaupp, M.; Marefat Khah, A.; Karbalaei Khani, S.; Müller, T.; Mack, F.; Nguyen, B. D.; Parker, S. M.; Perlt, E.; Rappoport, D.; Reiter, K.; Roy, S.; Rückert, M.; Schmitz, G.; Sierka, M.; Tapavicza, E.; Tew, D. P.; van Wüllen, C.; Voora, V. K.; Weigend, F.; Wodyński, A.; Yu, J. M. TURBOMOLE: Modular program suite for *ab initio* quantum-chemical and condensed-matter simulations. *J. Chem. Phys.* **2020**, *152*, 184107.

(97) Developers' version of TURBOMOLE V7.7 2021, a development of University of Karlsruhe and Forschungszentrum Karlsruhe GmbH, 1989-2007, TURBOMOLE GmbH,

since 2007; available from `https://www.turbomole.org` (retrieved November 29, 2022).

(98) Franzke, Y. J.; Middendorf, N.; Weigend, F. Efficient implementation of one- and two-component analytical energy gradients in exact two-component theory. *J. Chem. Phys.* **2018**, *148*, 104410.

(99) Visscher, L.; Dyall, K. G. Dirac-Fock atomic electronic structure calculations using different nuclear charge distributions. *At. Data Nucl. Data Tables* **1997**, *67*, 207–224.

(100) Franzke, Y. J. Calculation of NMR Parameters in a Modern Relativistic Density Functional Framework: Theory, Implementation, and Application. Dissertation, Karlsruhe Institute of Technology (KIT), Germany, 2021.

(101) OpenMP Architecture Review Boards, OpenMP API shared-memory parallel programming. `https://www.openmp.org` (retrieved September 26, 2021).

(102) Holzer, C.; Franzke, Y. J. OpenMP version of ridft, rdgrad, and egrad with contributions to mpshift, dscf, and grad; improved OpenMP version of aoforce and escf, released with TURBOMOLE V7.4 and further improved in TURBOMOLE V7.5.

(103) Peng, D.; Reiher, M. Local relativistic exact decoupling. *J. Chem. Phys.* **2012**, *136*, 244108.

(104) Peng, D.; Middendorf, N.; Weigend, F.; Reiher, M. An efficient implementation of two-component relativistic exact-decoupling methods for large molecules. *J. Chem. Phys.* **2013**, *138*, 184105.

(105) Becke, A. D. Density-functional exchange-energy approximation with correct asymptotic behavior. *Phys. Rev. A* **1988**, *38*, 3098–3100.

(106) Perdew, J. P. Density-functional approximation for the correlation energy of the inhomogeneous electron gas. *Phys. Rev. B* **1986**, *33*, 8822–8824.

(107) Dyall, K. G. Relativistic Quadruple-Zeta and Revised Triple-Zeta and Double-Zeta Basis Sets for the 4p, 5p, and 6p Elements. *Theor. Chem. Acc.* **2006**, *115*, 441–447.

(108) Basis sets available from the Dirac program web site, `http://dirac.chem.sdu.dk` (retrieved March 26, 2020).

(109) Jensen, F. The Basis Set Convergence of Spin–Spin Coupling Constants Calculated by Density Functional Methods. *J. Chem. Theory Comput.* **2006**, *2*, 1360–1369.

(110) Treutler, O.; Ahlrichs, R. Efficient molecular numerical integration schemes. *J. Chem. Phys.* **1995**, *102*, 346–354.

(111) Treutler, O. Entwicklung und Anwendung von Dichtefunktionalmethoden. Dissertation (Dr. rer. nat.), University of Karlsruhe (TH), Germany, 1995.

(112) Franzke, Y. J.; Treß, R.; Pazdera, T. M.; Weigend, F. Error-consistent segmented contracted all-electron relativistic basis sets of double- and triple-zeta quality for NMR shielding constants. *Phys. Chem. Chem. Phys.* **2019**, *21*, 16658–16664.

(113) Boettger, J. C. Approximate two-electron spin-orbit coupling term for density-functional-theory DFT calculations using the Douglas-Kroll-Hess transformation. *Phys. Rev. B* **2000**, *62*, 7809–7815.

(114) Filatov, M.; Zou, W.; Cremer, D. Spin-orbit coupling calculations with the two-component normalized elimination of the small component method. *J. Chem. Phys.* **2013**, *139*, 014106.

(115) Zou, W.; Filatov, M.; Cremer, D. Analytical energy gradient for the two-component normalized elimination of the small component method. *J. Chem. Phys.* **2015**, *142*, 214106.

(116) Pollak, P.; Weigend, F. Segmented Contracted Error-Consistent Basis Sets of Double-

and Triple-ζ Valence Quality for One- and Two-Component Relativistic All-Electron Calculations. *J. Chem. Theory Comput.* **2017**, *13*, 3696–3705.

(117) Eichkorn, K.; Treutler, O.; Öhm, H.; Häser, M.; Ahlrichs, R. Auxiliary Basis Sets to Approximate Coulomb Potentials. *Chem. Phys. Lett.* **1995**, *242*, 283–290.

(118) Eichkorn, K.; Weigend, F.; Treutler, O.; Ahlrichs, R. Auxiliary basis sets for main row atoms and transition metals and their use to approximate Coulomb potentials. *Theor. Chem. Acc.* **1997**, *97*, 119–124.

(119) Armbruster, M. K.; Weigend, F.; van Wüllen, C.; Klopper, W. Self-consistent treatment of spin-orbit interactions with efficient Hartree-Fock and density functional methods. *Phys. Chem. Chem. Phys.* **2008**, *10*, 1748–1756.

(120) Weigend, F.; Kattannek, M.; Ahlrichs, R. Approximated electron repulsion integrals: Cholesky decomposition versus resolution of the identity methods. *J. Chem. Phys.* **2009**, *130*, 164106.

(121) Klamt, A.; Schüürmann, G. COSMO: a new approach to dielectric screening in solvents with explicit expressions for the screening energy and its gradient. *J. Chem. Soc., Perkin Trans. 2* **1993**, 799–805.

(122) Schäfer, A.; Klamt, A.; Sattel, D.; Lohrenz, J. C. W.; Eckert, F. COSMO Implementation in TURBOMOLE: Extension of an efficient quantum chemical code towards liquid systems. *Phys. Chem. Chem. Phys.* **2000**, *2*, 2187–2193.

(123) Manual of TURBOMOLE V7.6 2021, a development of University of Karlsruhe and Forschungszentrum Karlsruhe GmbH, 1989-2007, TURBOMOLE GmbH, since 2007; available from `https://www.turbomole.org/turbomole/turbomole-documentation/` (retrieved January 12, 2022).

(124) Marques, M. A. L.; Oliveira, M. J. T.; Burnus, T. Libxc: A library of exchange and correlation functionals for density functional theory. *Comput. Phys. Commun.* **2012**, *183*, 2272–2281.

(125) Lehtola, S.; Steigemann, C.; Oliveira, M. J. T.; Marques, M. A. L. Recent developments in libxc – A comprehensive library of functionals for density functional theory. *SoftwareX* **2018**, *7*, 1–5.

(126) Libxc. Version 6.0.0 available from `https://www.tddft.org/programs/libxc/` (retrieved November 29, 2022).

(127) Perdew, J. P.; Burke, K.; Ernzerhof, M. Generalized Gradient Approximation Made Simple. *Phys. Rev. Lett.* **1996**, *77*, 3865–3868.

(128) Tao, J.; Perdew, J. P.; Staroverov, V. N.; Scuseria, G. E. Climbing the Density Functional Ladder: Nonempirical Meta–Generalized Gradient Approximation Designed for Molecules and Solids. *Phys. Rev. Lett.* **2003**, *91*, 146401.

(129) Zhao, Y.; Truhlar, D. G. A new local density functional for main-group thermochemistry, transition metal bonding, thermochemical kinetics, and noncovalent interactions. *J. Chem. Phys.* **2006**, *125*, 194101.

(130) Peverati, R.; Truhlar, D. G. M11-L: A Local Density Functional That Provides Improved Accuracy for Electronic Structure Calculations in Chemistry and Physics. *J. Phys. Chem. Lett.* **2012**, *3*, 117–124.

(131) Peverati, R.; Truhlar, D. G. An improved and broadly accurate local approximation to the exchange–correlation density functional: The MN12-L functional for electronic structure calculations in chemistry and physics. *Phys. Chem. Chem. Phys.* **2012**, *14*, 13171–13174.

(132) Yu, H. S.; He, X.; Truhlar, D. G. MN15-L: A New Local Exchange-Correlation Functional for Kohn–Sham Density Functional Theory with Broad Accuracy for Atoms, Molecules, and Solids. *J. Chem. Theory Comput.* **2016**, *12*, 1280–1293.

(133) Tao, J.; Mo, Y. Accurate Semilocal Density Functional for Condensed-Matter Physics and Quantum Chemistry. *Phys. Rev. Lett.* **2016**, *117*, 073001.

(134) Furness, J. W.; Kaplan, A. D.; Ning, J.; Perdew, J. P.; Sun, J. Accurate and Numerically Efficient r^{2}SCAN Meta-Generalized Gradient Approximation. *J. Phys. Chem. Lett.* **2020**, *11*, 8208–8215.

(135) Furness, J. W.; Kaplan, A. D.; Ning, J.; Perdew, J. P.; Sun, J. Correction to "Accurate and Numerically Efficient r^{2}SCAN Meta-Generalized Gradient Approximation". *J. Phys. Chem. Lett.* **2020**, *11*, 9248–9248.

(136) Lee, C.; Yang, W.; Parr, R. G. Development of the Colle-Salvetti correlation-energy formula into a functional of the electron density. *Phys. Rev. B* **1988**, *37*, 785–789.

(137) Becke, A. D. A new mixing of Hartree–Fock and local density-functional theories. *J. Chem. Phys.* **1993**, *98*, 1372–1377.

(138) Stephens, P. J.; Devlin, F. J.; Chabalowski, C. F.; Frisch, M. J. Ab Initio Calculation of Vibrational Absorption and Circular Dichroism Spectra Using Density Functional Force Fields. *J. Phys. Chem.* **1994**, *98*, 11623–11627.

(139) Adamo, C.; Barone, V. Toward reliable density functional methods without adjustable parameters: The PBE0 model. *J. Chem. Phys.* **1999**, *110*, 6158–6170.

(140) Staroverov, V. N.; Scuseria, G. E.; Tao, J.; Perdew, J. P. Comparative assessment of a new nonempirical density functional: Molecules and hydrogen-bonded complexes. *J. Chem. Phys.* **2003**, *119*, 12129–12137.

(141) Zhao, Y.; Truhlar, D. G. The M06 suite of density functionals for main group thermochemistry, thermochemical kinetics, noncovalent interactions, excited states, and transition elements: two new functionals and systematic testing of four M06-class functionals and 12 other functionals. *Theor. Chem. Acc.* **2008**, *120*, 215–241.

(142) Yu, H. S.; He, X.; Li, S. L.; Truhlar, D. G. MN15: A Kohn–Sham global-hybrid exchange–correlation density functional with broad accuracy for multi-reference and single-reference systems and noncovalent interactions. *Chem. Sci.* **2016**, *7*, 5032–5051.

(143) Bursch, M.; Neugebauer, H.; Ehlert, S.; Grimme, S. Dispersion corrected r^2SCAN based global hybrid functionals: r^2SCANh, r^2SCAN0, and r^2SCAN50. *J. Chem. Phys.* **2022**, *156*, 134105.

(144) Yanai, T.; Tew, D. P.; Handy, N. C. A new hybrid exchange–correlation functional using the Coulomb-attenuating method (CAM-B3LYP). *Chem. Phys. Lett.* **2004**, *393*, 51–57.

(145) Chai, J.-D.; Head-Gordon, M. Long-range corrected hybrid density functionals with damped atom–atom dispersion corrections. *Phys. Chem. Chem. Phys.* **2008**, *10*, 6615–6620.

(146) Mardirossian, N.; Head-Gordon, M. ωB97M-V: A combinatorially optimized, range-separated hybrid, meta-GGA density functional with VV10 nonlocal correlation. *J. Chem. Phys.* **2016**, *144*, 214110.

(147) Peverati, R.; Truhlar, D. G. Improving the Accuracy of Hybrid Meta-GGA Density Functionals by Range Separation. *J. Phys. Chem. Lett.* **2011**, *2*, 2810–2817.

(148) Verma, P.; Wang, Y.; Ghosh, S.; He, X.; Truhlar, D. G. Revised M11 Exchange-Correlation Functional for Electronic Excitation Energies and Ground-State Properties. *J. Phys. Chem. A* **2019**, *123*, 2966–2990.

(149) Peverati, R.; Truhlar, D. G. Screened-exchange density functionals with broad accuracy for chemistry and solid-state physics. *Phys. Chem. Chem. Phys.* **2012**, *14*, 16187–16191.

(150) Jaramillo, J.; Scuseria, G. E.; Ernzerhof, M. Local hybrid functionals. *J. Chem. Phys.* **2003**, *118*, 1068–1073.

(151) Maier, T. M.; Arbuznikov, A. V.; Kaupp, M. Local hybrid functionals: Theory, implementation, and performance of an emerging new tool in quantum chemistry and beyond. *Wiley Interdiscip. Rev.: Comput. Mol. Sci.* **2018**, *9*, e1378.

(152) Bahmann, H.; Rodenberg, A.; Arbuznikov, A. V.; Kaupp, M. A thermochemically competitive local hybrid functional without gradient corrections. *J. Chem. Phys.* **2007**, *126*, 011103.

(153) Arbuznikov, A. V.; Kaupp, M. Importance of the correlation contribution for local hybrid functionals: Range separation and self-interaction corrections. *J. Chem. Phys.* **2012**, *136*, 014111.

(154) Arbuznikov, A. V.; Kaupp, M. Towards improved local hybrid functionals by calibration of exchange-energy densities. *J. Chem. Phys.* **2014**, *141*, 204101.

(155) Haasler, M.; Maier, T. M.; Grotjahn, R.; Gückel, S.; Arbuznikov, A. V.; Kaupp, M. A Local Hybrid Functional with Wide Applicability and Good Balance between (De)Localization and Left–Right Correlation. *J. Chem. Theory Comput.* **2020**, *16*, 5645–5657.

(156) Perdew, J. P.; Staroverov, V. N.; Tao, J.; Scuseria, G. E. Density functional with full exact exchange, balanced nonlocality of correlation, and constraint satisfaction. *Phys. Rev. A* **2008**, *78*, 052513.

(157) Johnson, E. R. Local-hybrid functional based on the correlation length. *J. Chem. Phys.* **2014**, *141*, 124120.

(158) Holzer, C.; Franzke, Y. J. A Local Hybrid Exchange Functional Approximation from First Principles. *J. Chem. Phys.* **2022**, *157*, 034108.

(159) Plessow, P.; Weigend, F. Seminumerical calculation of the Hartree–Fock exchange matrix: Application to two-component procedures and efficient evaluation of local hybrid density functionals. *J. Comput. Chem.* **2012**, *33*, 810–816.

(160) Bahmann, H.; Kaupp, M. Efficient Self-Consistent Implementation of Local Hybrid Functionals. *J. Chem. Theory Comput.* **2015**, *11*, 1540–1548.

(161) Holzer, C. An improved seminumerical Coulomb and exchange algorithm for properties and excited states in modern density functional theory. *J. Chem. Phys.* **2020**, *153*, 184115.

(162) Franzke, Y. J.; Spiske, L.; Pollak, P.; Weigend, F. Segmented Contracted Error-Consistent Basis Sets of Quadruple-ζ Valence Quality for One- and Two-Component Relativistic All-Electron Calculations. *J. Chem. Theory Comput.* **2020**, *16*, 5658–5674.

(163) Balmer, M.; Franzke, Y. J.; Weigend, F.; von Hänisch, C. Low valent group 14 phosphinidenide complexes [$(SIDippP)_2M$] exhibit P-M pπ-pπ interaction (M = Ge, Sn, Pb). *Chem. Eur. J.* **2020**, *26*, 192–197.

(164) Caldeweyher, E.; Bannwarth, C.; Grimme, S. Extension of the D3 dispersion coefficient model. *J. Chem. Phys.* **2017**, *147*, 034112.

(165) Ehlert, S.; Huniar, U.; Ning, J.; Furness, J. W.; Sun, J.; Kaplan, A. D.; Perdew, J. P.; Brandenburg, J. G. r^2SCAN-D4: Dispersion corrected meta-generalized gradient approximation for general chemical applications. *J. Chem. Phys.* **2021**, *154*, 061101.

(166) Reimann, M.; Kaupp, M. Spin-State Splittings in 3d Transition-Metal Complexes Revisited: Benchmarking Approximate Methods for Adiabatic Spin-State Energy Differences in Fe(II) Complexes. *J. Chem. Theory Comput.* **2022**, DOI: 10.1021/acs.jctc.2c00924.

(167) Krätschmer, F.; Sun, X.; Gillhuber, S.; Kucher, H.; Franzke, Y. J.; Weigend, F.; Roesky, P. Fully tin coated coinage metal ions — A pincer type bis-stannylene ligand for exclusive tetrahedral complexation. *Chem. Eur. J* **2022**, accepted.

(168) Weigend, F.; Ahlrichs, R. Balanced basis sets of split valence, triple zeta valence and quadruple zeta valence quality for H to Rn: Design and assessment of accuracy. *Phys. Chem. Chem. Phys.* **2005**, *7*, 3297–3305.

(169) Ahlrichs, R.; May, K. Contracted all-electron Gaussian basis sets for atoms Rb to Xe. *Phys. Chem. Chem. Phys.* **2000**, *2*, 943–945.

(170) Sierka, M.; Hogekamp, A.; Ahlrichs, R. Fast evaluation of the Coulomb potential for electron densities using multipole accelerated resolution of identity approximation. *J. Chem. Phys.* **2003**, *118*, 9136–9148.

(171) NMR SSCCs with the ReSpect program suite, `http://www.respectprogram.org/nmr-sscc.html` (retrieved December 2, 2022).

(172) Raynes, W. T.; Geertsen, J.; Oddershede, J. Unexpected differential sensitivity of nuclear spin–spin coupling constants to bond stretching in methane. *Chem. Phys. Lett.* **1992**, *197*, 516–524.

(173) Fowler, P. Vibration-rotation effects on properties of symmetric tops and linear molecules. *Mol. Phys.* **1981**, *43*, 591–600.

(174) Wilkins, A. L.; Watkinson, P. J.; Mackay, K. M. Aspects of germanium-73 nuclear magnetic resonance spectroscopy. *J. Chem. Soc., Dalton Trans.* **1987**, 2365–2372.

(175) Dreeskamp, H. Indirekte Kernspinkopplung zwischen Protonen und Elementen der IV. Gruppe. *Z. Naturforsch. A* **1964**, *19*, 139–142.

(176) McFarlane, W. Heteronuclear double resonance: ^{119}Sn–^{13}C spin–spin coupling in organotin compounds. *J. Chem. Soc. A* **1967**, 528–530.

(177) Petrosyan, V.; Permin, A.; Reutov, O.; Roberts, J. D. The ^{119}Sn–^{13}C and ^{119}Sn–^{1}H couplings for methyl derivatives of tin in various solvents. *J. Magn. Reson.* **1980**, *40*, 511–518.

(178) Petrosyan, V. NMR Spectra and structures of organotin compounds. *Prog. Nucl. Magn. Reson. Spectrosc.* **1977**, *11*, 115–148.

(179) Schumann, C.; Dreeskamp, H. Geminal spin coupling constants in group IV hydrides investigated by double resonance. *J. Magn. Reson.* **1970**, *3*, 204–217.

(180) McFarlane, W. A heteronuclear magnetic double resonance study of hexamethylditin. *J. Chem. Soc. A* **1968**, 1630–1634.

(181) Birchall, T.; Pereira, A. The ^{1}H nuclear magnetic resonance spectrum of the stannyl ion. *J. Chem. Soc., Chem. Commun.* **1972**, 1150–1151.

(182) Dobson, J. F. Alternative expressions for the Fermi hole curvature. *J. Chem. Phys.* **1993**, *98*, 8870–8872.

(183) Becke, A. D. Current density in exchange-correlation functionals: Application to atomic states. *J. Chem. Phys.* **2002**, *117*, 6935–6938.

(184) Tao, J. Explicit inclusion of paramagnetic current density in the exchange-correlation functionals of current-density functional theory. *Phys. Rev. B* **2005**, *71*, 205107.

(185) Holzer, C.; Franzke, Y. J.; Pausch, A. Current density functional framework for spin–orbit coupling. *J. Chem. Phys.* **2022**, *157*, 204102.

(186) Franzke, Y. J.; Yu, J. M. Hyperfine Coupling Constants in Local Exact Two-Component Theory. *J. Chem. Theory Comput.* **2022**, *18*, 323–343.

(187) Franzke, Y. J.; Yu, J. M. Quasi-Relativistic Calculation of EPR g Tensors with Derivatives of the Decoupling Transformation, Gauge-Including Atomic Orbitals, and Magnetic Balance. *J. Chem. Theory Comput.* **2022**, *18*, 2246–2266.

(188) Lichtenberger, N.; Franzke, Y. J.; Massa, W.; Weigend, F.; Dehnen, S. The Identity of "Ternary" A/Tl/Pb or K/Tl/Bi Solid Mixtures and Binary Zintl Anions Isolated From Their Solutions. *Chem. Eur. J.* **2018**, *24*, 12022–12030.

(189) Eulenstein, A. R.; Franzke, Y. J.; Bügel, P.; Massa, W.; Weigend, F.; Dehnen, S. Stabilizing a metalloid $\{Zn_{12}\}$ unit within a polymetallide environment in $[K_2Zn_{20}Bi_{16}]^{6-}$. *Nat. Commun.* **2020**, *11*, 5122.

(190) Eulenstein, A. R.; Franzke, Y. J.; Lichtenberger, N.; Wilson, R. J.; Deubner, H. L.; Kraus, F.; Weigend, F.; Dehnen, S. Substantial π-aromaticity of the anionic heavy-metal cluster $[Th@Bi_{12}]^{4-}$. *Nat. Chem.* **2021**, *13*, 149–155.

(191) Weigend, F. A fully direct RI-HF algorithm: Implementation, optimised auxiliary basis sets, demonstration of accuracy and efficiency. *Phys. Chem. Chem. Phys.* **2002**, *4*, 4285–4291.

(192) Baldes, A.; Weigend, F. Efficient two-component self-consistent field procedures and gradients: implementation in TURBOMOLE and application to Au_{20}^-. *Mol. Phys.* **2013**, *111*, 2617–2624.

(193) Neese, F.; Wennmohs, F.; Hansen, A.; Becker, U. Efficient, approximate and parallel Hartree–Fock and hybrid DFT calculations. A 'chain-of-spheres' algorithm for the Hartree–Fock exchange. *Chem. Phys.* **2009**, *356*, 98–109.

(194) Stoychev, G. L.; Auer, A. A.; Izsák, R.; Neese, F. Self-Consistent Field Calculation of Nuclear Magnetic Resonance Chemical Shielding Constants Using Gauge-Including Atomic Orbitals and Approximate Two-Electron Integrals. *J. Chem. Theory Comput.* **2018**, *14*, 619–637.

(195) Friesner, R. A. Solution of self-consistent field electronic structure equations by a pseudospectral method. *Chem. Phys. Lett.* **1985**, *116*, 39–43.

(196) Friesner, R. A. Solution of the Hartree–Fock equations by a pseudospectral method: Application to diatomic molecules. *J. Chem. Phys.* **1986**, *85*, 1462–1468.

(197) Friesner, R. A. Solution of the Hartree–Fock equations for polyatomic molecules by a pseudospectral method. *J. Chem. Phys.* **1987**, *86*, 3522–3531.

(198) Ringnalda, M. N.; Belhadj, M.; Friesner, R. A. Pseudospectral Hartree–Fock theory: Applications and algorithmic improvements. *J. Chem. Phys.* **1990**, *93*, 3397–3407.

(199) Martinez, T. J.; Carter, E. A. Pseudospectral methods applied to the electron correlation problem. In *Modern Electronic Structure Theory – Part II*; Yarkony, D. R., Ed.; World Scientific Press: Singapore, 1995; Chapter 17, pp 1132–1165.

(200) Weigend, F.; Häser, M.; Patzelt, H.; Ahlrichs, R. RI-MP2: optimized auxiliary basis sets and demonstration of efficiency. *Chem. Phys. Lett.* **1998**, *294*, 143–152.

(201) Jensen, F. Basis Set Convergence of Nuclear Magnetic Shielding Constants Calculated by Density Functional Methods. *J. Chem. Theory Comput.* **2008**, *4*, 719–727.

(202) Jensen, F. Segmented Contracted Basis Sets Optimized for Nuclear Magnetic Shielding. *J. Chem. Theory Comput.* **2015**, *11*, 132–138.

(203) Benedikt, U.; Auer, A. A.; Jensen, F. Optimization of augmentation functions for correlated calculations of spin-spin coupling constants and related properties. *J. Chem. Phys.* **2008**, *129*, 064111.

(204) Weigend, F.; Baldes, A. Segmented contracted basis sets for one- and two-component Dirac-Fock effective core potentials. *J. Chem. Phys.* **2010**, *133*, 174102.

(205) Hill, J. G. Gaussian basis sets for molecular applications. *Int. J. Quantum Chem.* **2013**, *113*, 21–34.

(206) Jensen, F. Atomic orbital basis sets. *Wiley Interdiscip. Rev.: Comput. Mol. Sci.* **2013**, *3*, 273–295.

(207) Weigend, F. Error-Balanced Segmented Contracted Gaussian Basis Sets. In *Computational Methods in Lanthanide and Actinide Chemistry*; John Wiley & Sons, Chichester, United Kingdom, 2015; Chapter 7, pp 181–194.

(208) Peterson, K. A.; Dyall, K. G. Gaussian Basis Sets for Lanthanide and Actinide Elements. In *Computational Methods in Lanthanide and Actinide Chemistry*; John Wiley & Sons, Chichester, United Kingdom, 2015; Chapter 8, pp 195–216.

(209) Sherrill, C. D.; Manolopoulos, D. E.; Martínez, T. J.; Michaelides, A. Electronic structure software. *J. Chem. Phys.* **2020**, *153*, 070401.